

REPUBLIQUE ALGERIENNE DEMOCRATIQUE ET POPULAIRE
MINISTRE DE L'ENSEIGNEMENT SUPERIEUR ET DE LA RECHERCHE

SCIENTIFIQUE

Université de Mohamed El-Bachir El-Ibrahimi - Bordj Bou Arreridj

Faculté des Sciences et de la technologie

Département d'Electronique

Mémoire

Présenté pour obtenir

LE DIPLOME DE MASTER

FILIERE : Electronique

Spécialité : Industrie Electronique

Par

- Mansouri Houssam Eddine
- Lahbous Mohammed

Intitulé

Commande directe du couple de deux moteurs asynchrones alimentés par un onduleur à neuf (09) interrupteurs

Évalué le :

Par la commission d'évaluation composée de* :

Nom & Prénom	Grade	Qualité	Etablissement
M.BOUKEZATA Boualem	MCB	Président	Univ-BBA
M.TALBI Billel	MCB	Encadreur	Univ-BBA
M.BENTOUHAMI Larafi	MCB	Examineur	Univ-BBA

Année Universitaire 2020/2021

* Conformément à :

- L'arrêté n°055 du 21 janvier 2021 Fixant dispositions exceptionnelles autorisées en matière d'organisation et gestion pédagogique, de l'évaluation et de la progression des étudiants, durant la période COVID-19 au titre de l'année universitaire 2020-2021 ;
- Procès-verbal de la réunion de l'équipe du domaine des Sciences et Technologies du mois de Mai 2021.

PEOPLE'S DEMOCRATIC REPUBLIC OF ALGERIA
MINISTRY OF HIGHER EDUCATION AND SCIENTIFIC RESEARCH

University Mohamed El-Bachir El-Ibrahimi - Bordj Bou Arreridj

Faculty of Science and Technology

Department of Electronics

Dissertation

Submitted in Partial Fulfillment of the Requirement

for an ACADEMIC MASTER DEGREE

FIELD: Electronic

Specialty: Electronic Industry

Submitted by:

- **Mansouri Houssam Eddine**
- **Lahbous Mohammed**

Titled

***Direct Torque Control of Two Induction Motors using the Nine-Switch
inverter***

Evaluated on:

By the evaluation committee composed of:*

<i>Last & First name</i>	<i>Grade</i>	<i>Quality</i>	<i>Establishment</i>
<i>M.BOUKEZATA Boualem</i>	<i>MCB</i>	<i>President</i>	<i>Univ-BBA</i>
<i>M.TALBI Billel</i>	<i>MCB</i>	<i>Supervisor</i>	<i>Univ-BBA</i>
<i>M.BENTOUHAMI Larafi</i>	<i>MCB</i>	<i>Examiner</i>	<i>Univ-BBA</i>

Academic Year 2020/2021

* In accordance with:

- Decree n ° 055 of January 21, 2021 Fixing exceptional authorized provisions in terms of organization and pedagogical management, evaluation and progression of students, during the COVID-19 period for the academic year 2020- 2021;
- Record of the meeting of the Science and Technology team for the month of May 2021.

Acknowledgments

*Praise be to Allah, Lord of the Worlds, and prayers and peace be upon the
Messenger of Allah.*

*We would like to articulate our deep and sincere gratitude to our
supervisor **Dr. Billel Talbi** for his invaluable timely guidance and
support and who have always been our motivation for carrying out
this work, which could not have been completed without him. His
vision, sincerity and motivation have deeply inspired us. It was a
great privilege and honor to study and work under his guidance.*

My god bless him and his family.

*A debt of gratitude is owed to all the people who contributed in any
manner to the work described here.*

Table of contents

Acknowledgments.....	I
Table of contents	II
List of figures	IV
List of Tables	IV
Acronyms	VI
Nomenclature	VII
General Introduction	1
Chapter I: Modeling of Induction Motor Fed from Voltage Source Inverters.....	2
I.1 INTRODUCTION	2
I.2 INDUCTION MOTOR.....	2
I.2.1. STRUCTURE AND BASIC OPERATION PRINCIPLE.....	2
I.2.2. INDUCTION MOTOR MODELING.....	4
I.2.2.1 <i>VOLTAGE EQUATIONS</i>	4
I.2.2.2 <i>FLUX EQUATIONS</i>	5
I.2.2.3 <i>MECHANICAL EQUATIONS</i>	5
I.2.2.4 <i>PARK TRANSFORMATION</i>	6
I.3. VOLTAGE SOURCE INVERTERS	7
I.3.1. SIX-SWITCH VOLTAGE SOURCE INVERTER	7
I.3.2. NINE-SWITCH VOLTAGE SOURCE INVERTER	9
I.4. BACKGROUND ON INDUCTION MOTOR DRIVES	11
I.5 CONCLUSION.....	12
Chapter II: Direct Torque Control of Induction Motor	13
II.1 INTRODUCTION	13
II.2. PRINCIPAL OF DIRECT TORQUE CONTROL	13
II.3. CONTROL OF STATOR FLUX AND ELECTROMAGNETIC TORQUE.....	14
II.3.1. CONTROL OF STATOR FLUX	14
II.3.2. CONTROL OF ELECTROMAGNETIC TORQUE	16

II.4. ESTIMATION OF STATOR FLUX AND ELECTROMAGNETIC TORQUE	17
II.4.1. STATOR FLUX ESTIMATION	17
II.4.2. ELECTROMAGNETIC TORQUE ESTIMATION	18
II.5. SWITCHING TABLE CONSTRUCTION	18
II.6. SPEED REGULATION	19
II.7. SIMULATION RESULTS	20
II.8 CONCLUSION	25
Chapter III: Direct Torque Control of two Induction Motors	26
III.1. INTRODUCTION	26
III.2. STRUCTURE WITH TWO SIX-SWITCH VOLTAGE SOURCE INVERTERS	27
III.2.1. CONTROL SCHEME	27
III.2.2. SIMULATION RESULTS	28
III.3. STRUCTURE WITH NINE-SWITCHES VOLTAGE SOURCE INVERTER	32
III.3.1. CONTROL SCHEME	33
III.3.2. SIMULATION RESULTS	35
III.4. COMPARATIVE STUDY	39
III.5. CONCLUSION	42
General Conclusion	43
Appendix	44
References	45
Abstract	

List of figures

Figure I.1 Induction Motor general structure	3
Figure I.2 Production of rotating magnetic field in the stator.	4
Figure I.3 Angles between electric frames.....	7
Figure I.4 Three-phase inverter (six switches).....	8
Figure I.5 Different voltage vectors generated by a six-switch inverter	8
Figure I.6 (a) The classical Dual output inverter, (b) nine-switch inverter.	9
Figure I.7 AC motor control schemes.	12
Figure II.1 Basic DTC bloc diagram.	14
Figure II.2 Evolution of stator flux vector in the complex plan.	15
Figure II.3 Two-level hysteresis comparator for stator flux control.....	16
Figure II.4 Three-level hysteresis comparator for electromagnetic torque control.	17
Figure II.5 Speed anti-windup PI controller.	20
Figure II.6 Simulink block diagram of the developed DTC.	20
Figure II.7 Simulation results of DTC for No-load start followed by load disturbances.	23
Figure II.8 Simulation results of DTC for Reversed Rotation.....	25
Figure III.1 Six-phase VSI connected to dual three-phase IM	27
Figure III.2 DTC control scheme when applied to the DTLI.	28
Figure III.3 Simulink model of DTC with six-phase VSI	29
Figure III.4 Simulation results of DTC with six-phase VSI for several speed combinations coupled with nominal loads.	32
Figure III.5 Block diagram of DTC with NSI.	33
Figure III.6 Flowchart of the suggested algorithm.	34
Figure III.7 Voltage space vector locations.	34
Figure III.8 Simulink model of the synchronization block.	35
Figure III.9 Developed simulation model of DTC with NSI	36
Figure III.10 Simulation results of DTC with NSI for several speed combinations coupled with nominal loads.	39

List of Tables

Table I.1 NSI leg states	10
Table I.2 NSI leg states and their corresponding Voltage space vectors $V_x V_y$	11
Table II.1 Generalized switching table.	19
Table II.2 Optimum voltage vector look-up table.....	19
Table III.1 Comparison between both approaches Motor 01 (Blue).	40
Table III.2 Comparison between both approaches Motor 02 (Green).	41
Table A.1 Parameters of the induction machine	44

Acronyms

AC	Alternative Current.
DC	Direct Current.
IM	Induction Motor.
EMF	Electro-Motive Force.
VSI	Voltage Source Inverter.
NSI	Nine-Switch Inverter.
XOR	logic operation gate Exclusive OR.
DTC	Direct Torque Control.
PI	Proportional-Integral.
FLI	Five-Leg Inverter
THD	Total Harmonic Distortion.
SVM	Space vector modulation.
IGBT	insulated-gate bipolar transistor.
FOC	Field oriented control.
VFD	Variable-frequency drive.
PWM	Pulse Width Modulation.

Nomenclature

v_{sabc}	Vector of the stator voltages
i_{sabc}	Vector of the stator currents
v_{rabc}	Vector of the rotor voltages
i_{rabc}	Vector of the rotor currents
ϕ_{sabc}	Vector of the stator flux
ϕ_{rabc}	Vector of the rotor flux
R_s, R_r	Stator and Rotor resistances respectively
l_s, l_r	Self-inductances of the stator and the rotor respectively
L_{os}, L_{or}	Stator and rotor inductances respectively.
M_{os}	Mutual inductance between two stator phases.
M_{or}	Mutual inductance between two rotor phases.
M_{osr}	Stator-Rotor mutual inductance.
L_s, L_r	Stator-Rotor cyclical inductance respectively
P	Number of poles pairs.
θ	Angle position between the stator and the rotor.
ω_m	Rotor speed
T_{em}	Electromagnetic motor torque
T_L	Load torque
T_d	Dry torque
J	Inertia moment.
F	Viscous friction coefficient.
W_{mag}	Magnetic energy.
ψ	Angle between the stationary reference frame and the rotating reference frame
V_{dc}	DC-bus voltage.
S_K	Switch mode
V_x, V_y	voltage space vector of the upper and the lower ‘sub-inverter’ respectively
$i_{s\alpha}, i_{s\beta}$	α and β components of stator currents.
$v_{s\alpha}, v_{s\beta}$	α and β components of stator voltage.
$\phi_{s\alpha}, \phi_{s\beta}$	α and β components of stator flux.
h_{ϕ_s}	Hysteresis band of stator flux.
h_{T_e}	Hysteresis band of stator torque.

General Introduction

Industrial applications require large numbers of motors; therefore, it is necessary to design systems with low cost, reduced losses and higher efficiency. As a substitution to two conventional two-level inverters, the Nine-Switch Inverter (NSI) should be a good candidate for the use in various industrial applications. Thanks to its special topology with reduced number of semiconductor switches, it can be used to drive two three-phase loads independently. On the other hand, the Direct Torque Control (DTC) is a robust control scheme of AC motors, which consist of selecting proper state vectors of a conventional voltage source inverter.

The NSI, having a different working principle from the conventional voltage source inverter and taking into account the varying influence of active space vectors on the motor's torque and stator flux.

In this context, a Direct Torque Control method is suggested to, efficiently, drive two induction motors independently, while keeping torque and stator flux ripples in permissible ranges. Simulations are carried-out to show that the developed independent control is effective and provides a simple configuration with high performance in terms of speed and torque responses.

The details description of this project is compiled into 3 chapters:

- Chapter I: deals with a general background about three-phase induction motor, voltage source inverters booth six-switch and nine-switch and AC motor control methods.
- Chapter II: describes basic principles of operation of the direct torque control, and estimation and control of booth flux and torque and ending up this chapter with simulation, which insures the validity of DTC.
- Chapter III: is aimed at direct torque control method used for two induction motors fed by nine-switch inverter with simulation results followed by discussion and comparative study between the NSI and conventional voltage source inverter. Finally, a general conclusion of this work and perspectives are listed at the end.

Chapter I:

Modeling of Induction Motor Fed from Voltage Source Inverters

I.1 INTRODUCTION

AC motors are invading into the application areas of motor drive whether being domestic application or industry. Variable frequency power supplies have freed AC motors from the fixed synchronous speed, and they have become adjustable speed motors. Among all the types of AC machines, the squirrel cage induction motor is widely used in industry because of its advantages: good self-starting capability, simple construction, low cost, reliable and need less maintenance etc.

The objective of this chapter is to present and model the induction motor, the six-switch and nine-switch voltage inverters, also to give a brief summary on the control techniques of the induction motor.

I.2 INDUCTION MOTOR

Induction motor (IM) is used for converting electrical energy into mechanical energy. It was invented by Nikola Tesla in the nineteenth century and exist in two main types, squirrel cage and wound rotor [1].

I.2.1. STRUCTURE AND BASIC OPERATION PRINCIPLE

The three-phase induction electric motor, as well as any electric motor, consists of two main parts: the stator (stationary part) and the rotor (rotating part), as presented in Figure I.1. Usually, the rotor is located inside the stator. There is a small distance between the rotor and the stator, called an air gap.

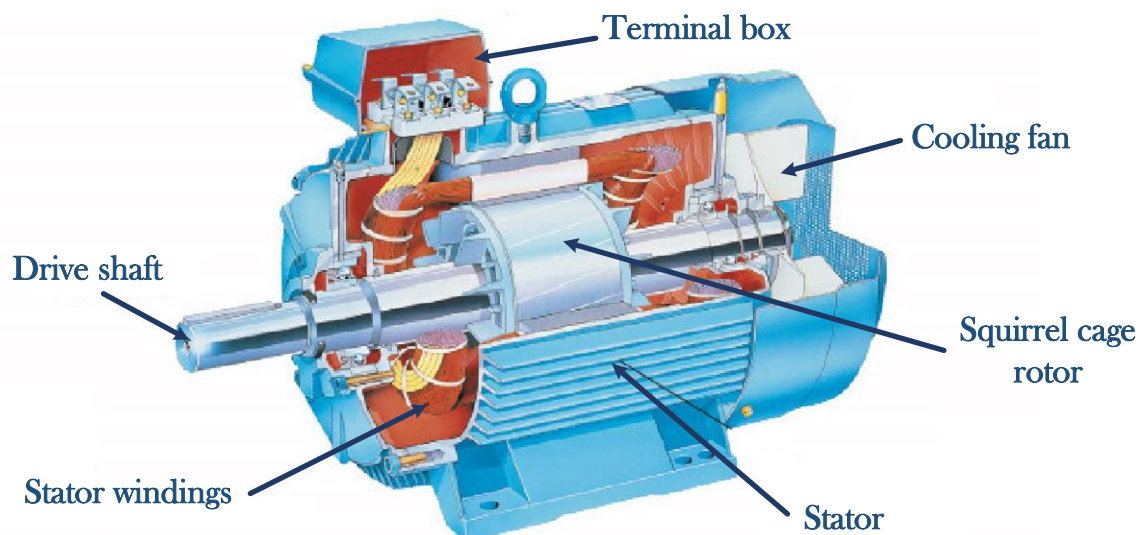


Figure I.1. Induction motor general structure.

The stator consists of an outer frame and a core with windings. The stator core is assembled from thin-sheet steel, usually 0.5 mm thick, covered with insulating varnish. Stator core laminations significantly limit the eddy current losses. The stator windings are located in the slots of the core. The rotor consists of a core with a short-circuited winding and a shaft. The rotor core also has a laminated construction. In this case, the rotor core sheets are not varnished, since the current has a small frequency and the oxide film is sufficient to limit the eddy currents [2].

The principle of operation of a three-phase induction motor is based on the ability of a three-phase winding to create a rotating magnetic field when it is connected to a three-phase electric power system. The speed of rotation of this field or synchronous speed is directly proportional to the supply frequency (f), and inversely proportional to the number of pairs of poles (p) of the three-phase winding $\omega_s = (4 \cdot \pi \cdot f) / p$ (rad/s) [3]. According to the Faraday's law of induction when the magnetic flux lines in the air gap cut both stator and rotor (being stationary, as the motor speed is zero) conductors at the same speed. An electromotive force (EMF) is induced in the rotor conductors due to the relative speed difference between the rotating flux and rotor conductors. The frequency of the induced EMF is the same as the supply frequency. Its magnitude is proportional to the relative velocity between the flux and the conductors. Since the rotor bars are shorted at the ends, the EMF induced produces a current in the rotor conductors. The direction of the rotor current opposes the relative velocity between rotating flux produced by the stator and stationary rotor conductors. The rotor starts rotating in the same direction as that of rotating magnetic field and tries to catch up with it. However, in

practice, the rotor never succeeds in catching up to the stator field. So, the rotor runs slower than the synchronous speed. This difference in speed is called slip speed. This slip speed depends upon the mechanical load on the motor shaft [3].

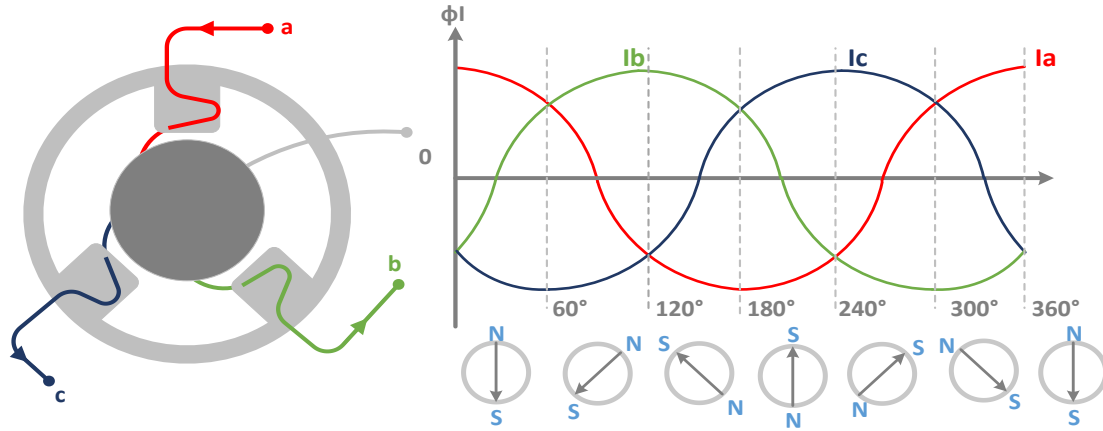


Figure I.2. Production of rotating magnetic field in the stator.

I.2.2. INDUCTION MOTOR MODELING

The modeling process consists of applying the electromagnetic laws to the different windings and motion equations to the rotor carrying the load.

I.2.2.1 VOLTAGE EQUATIONS

The stator and rotor voltage equations are given by the following two equations [4]:

$$[v_{sabc}] = [R_s][i_{sabc}] + \frac{d}{dt}[\phi_{sabc}] \quad (I.1)$$

$$0 = [v_{rabc}] = [R_r][i_{rabc}] + \frac{d}{dt}[\phi_{rabc}] \quad (I.2)$$

where $[v_{sabc}] = \begin{bmatrix} v_{sa} \\ v_{sb} \\ v_{sc} \end{bmatrix}$ is the vector of the stator voltages, $[v_{rabc}] = \begin{bmatrix} v_{ra} \\ v_{rb} \\ v_{rc} \end{bmatrix} = \begin{bmatrix} 0 \\ 0 \\ 0 \end{bmatrix}$ is the vector of

the rotor voltages, $[i_{sabc}] = \begin{bmatrix} i_{sa} \\ i_{sb} \\ i_{sc} \end{bmatrix}$ is the vector of the stator currents, $[i_{rabc}] = \begin{bmatrix} i_{ra} \\ i_{rb} \\ i_{rc} \end{bmatrix}$ is the vector

of the rotor currents, $[\phi_{sabc}] = \begin{bmatrix} \phi_{sa} \\ \phi_{sb} \\ \phi_{sc} \end{bmatrix}$: the vector of the stator flux, $[\phi_{rabc}] = \begin{bmatrix} \phi_{ra} \\ \phi_{rb} \\ \phi_{rc} \end{bmatrix}$ is the vector

of the rotor flux, $[R_s] = \begin{bmatrix} R_s & 0 & 0 \\ 0 & R_s & 0 \\ 0 & 0 & R_s \end{bmatrix}$ and $[R_r] = \begin{bmatrix} R_r & 0 & 0 \\ 0 & R_r & 0 \\ 0 & 0 & R_r \end{bmatrix}$ are the resistance matrices of

the stator and the rotor respectively.

I.2.2.2 FLUX EQUATIONS

Assuming a linear magnetic path, the stator and rotor flux equations can be expressed by the following two equations [4]:

$$[\phi_{sabc}] = [L_{os}][i_{sabc}] + [M_{osr}][i_{rabc}] \quad (\text{I.3})$$

$$[\phi_{rabc}] = [L_{or}][i_{rabc}] + [M_{osr}][i_{sabc}] \quad (\text{I.4})$$

where $[L_{os}] = \begin{bmatrix} l_s & M_{os} & M_{os} \\ M_{os} & l_s & M_{os} \\ M_{os} & M_{os} & l_s \end{bmatrix}$ and $[L_{or}] = \begin{bmatrix} l_r & M_{or} & M_{or} \\ M_{or} & l_r & M_{or} \\ M_{or} & M_{or} & l_r \end{bmatrix}$ are the inductance matrices of

the stator and the rotor respectively. l_s and l_r are the self-inductances, M_{os} is the mutual inductance between two stator phases, and M_{or} is the mutual inductance between two rotor

phases. $[M_{osr}] = M \begin{bmatrix} \cos(p\theta) & \cos\left(p\theta + \frac{2\pi}{3}\right) & \cos\left(p\theta + \frac{4\pi}{3}\right) \\ \cos\left(p\theta + \frac{4\pi}{3}\right) & \cos(p\theta) & \cos\left(p\theta + \frac{2\pi}{3}\right) \\ \cos\left(p\theta + \frac{4\pi}{3}\right) & \cos\left(p\theta + \frac{2\pi}{3}\right) & \cos(p\theta) \end{bmatrix}$ is the mutual

inductance matrix between the stator and the rotor. M presents the maximal mutual inductance between the stator phase and the rotor phase, p designates the number of pole pairs and θ denotes the position between the stator and the rotor.

I.2.2.3 MECHANICAL EQUATIONS

The rotor motion undergoes the following usual second order differential equation:

$$J \frac{d\omega_m}{dt} = -F\omega_m + T_{em} + T_L - T_d \quad (\text{I.5})$$

where ω_m , T_L , T_{em} , and T_d are, respectively, the rotor speed, the load torque, the electromagnetic motor torque, and the dry torque. J designates the inertia of the rotor-load set, and F the viscous friction coefficient.

The expression of T_{em} is obtained from the energy balance. Specifically, one has

$$T_{em} = \frac{\partial W_{mag}}{\partial \theta} \quad \text{with} \quad W_{mag} = \frac{1}{2} \left([i_{sabc}]^T [\phi_{sabc}] + [i_{rabc}]^T [\phi_{rabc}] \right) \quad (\text{I.6})$$

where W_{mag} denotes the magnetic energy. The induction motor model, including the equations (I.1), (I.2), and (I.5), entails a difficulty. Which is the system order is relatively large and to overcome this difficulty, adequate coordinate transformation is available that reduce the system order that is the PARK transformation.

I.2.2.4 PARK TRANSFORMATION

Using the overall Park transformation, the electrical equations of a three-phase model (stationary (a, b, c) frame) of the motor are transformed into the two-phase model (rotatory (d, q, 0) frame). The (d, q, 0) transformation can reduce three AC variables (voltages, currents ...) to two DC variables (Figure I.3). A general representation of the Park transformation is given

$$\text{as: } \begin{bmatrix} X_d \\ X_q \\ X_0 \end{bmatrix} = [P(\psi)] \begin{bmatrix} X_d \\ X_q \\ X_0 \end{bmatrix} \quad (\text{I.7})$$

with ψ is the angle between the stator phase axis of the stationary reference frame and the d axis of the rotating reference frame. Two different Park transformations can be defined: one preserving the amplitude the other preserving power; the later will be the focus of this study and is given as:

$$[Po(\psi)] = \sqrt{\frac{2}{3}} \begin{bmatrix} \cos(\omega) & \cos\left(\omega - \frac{2\pi}{3}\right) & \cos\left(\omega + \frac{2\pi}{3}\right) \\ \sin(\omega) & \sin\left(\omega - \frac{2\pi}{3}\right) & \sin\left(\omega + \frac{2\pi}{3}\right) \\ \frac{1}{\sqrt{2}} & \frac{1}{\sqrt{2}} & \frac{1}{\sqrt{2}} \end{bmatrix} \quad (\text{I.8})$$

and its inverse is given as:

$$[Po(\psi)]^{-1} = \sqrt{\frac{2}{3}} \begin{bmatrix} \cos(\omega) & \sin(\omega) & 1 \\ \cos\left(\omega - \frac{2\pi}{3}\right) & \sin\left(\omega - \frac{2\pi}{3}\right) & 1 \\ \cos\left(\omega + \frac{2\pi}{3}\right) & \sin\left(\omega + \frac{2\pi}{3}\right) & 1 \end{bmatrix} \quad (\text{I.9})$$

Applying the Park transformation to the induction machine equations (I.1) and (I.2) yields the following (d, q) equations:

$$\begin{cases} v_{sd} = R_s i_{sd} + \frac{d\phi_{sd}}{dt} - \frac{d\theta_s}{dt} \phi_{sd} \\ v_{sq} = R_s i_{sq} + \frac{d\phi_{sq}}{dt} + \frac{d\theta_s}{dt} \phi_{sq} \end{cases} \quad (\text{I.10})$$

$$\begin{cases} v_{rd} = 0 = R_r i_{rd} + \frac{d\phi_{rd}}{dt} - \left(\frac{d\theta_r}{dt} \phi_{rd} - p \frac{d\theta}{dt}\right) \phi_{rd} \\ v_{rq} = 0 = R_r i_{rq} + \frac{d\phi_{rq}}{dt} + \left(\frac{d\theta_r}{dt} \phi_{rq} - p \frac{d\theta}{dt}\right) \phi_{rq} \end{cases} \quad (\text{I.11})$$

Where $\psi = \theta_s$, for the transformation of stator variables, $\psi = \theta_r = \theta_s - \theta$, for the transformation of the rotor variables. Similarly, the obtained flux equations in the (d, q) frame can be given the more compact form:

$$\begin{cases} \left[\phi_{rdq} \right] = L_r \left[i_{rdq} \right] + L_m \left[i_{sdq} \right] \\ \left[\phi_{sdq} \right] = L_s \left[i_{sdq} \right] + L_m \left[i_{rdq} \right] \end{cases} \quad (\text{I.14})$$

With $L_s = l_s - L_{os}$ cyclical stator inductance; $L_r = l_r - L_{or}$ cyclical rotor inductance; $L_m = \frac{3}{2} M$, mutual inductance between the stator and rotor windings.

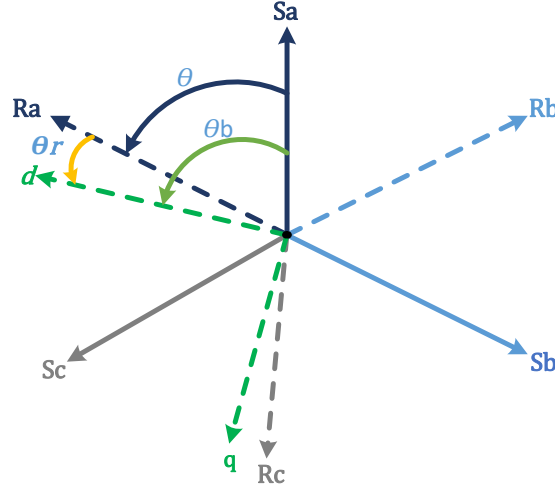


Figure I.3. Angles between electric frames.

I.3. VOLTAGE SOURCE INVERTERS

Voltage source inverter (VSI) is mainly used to convert a constant DC voltage into an AC voltage with variable magnitude and frequency.

I.3.1. SIX-SWITCH VOLTAGE SOURCE INVERTER

Figure I.4 shows the power circuit of a three-phase voltage source inverter. The leg voltages are denoted by V_A, V_B, V_C where the relationship between the leg voltage and switching signals is:

$$V_K = (S_K - 0.5)V_{dc} \quad K \in (A, B, C) \quad (\text{I.15})$$

where $S_K = 1$ when the upper power switch is 'ON' and $S_K = 0$ when the lower switch is 'ON' to avoid shorting the DC rail the upper and the lower switches are complimentary. Assuming ideal conditions, the relation between the phase-to-neutral load voltage and the leg voltages can be written as:

$$\begin{bmatrix} V_A \\ V_B \\ V_C \end{bmatrix} = \begin{bmatrix} 1 & 0 & 0 \\ 0 & 1 & 0 \\ 0 & 0 & 1 \end{bmatrix} \begin{bmatrix} v_{an} \\ v_{bn} \\ v_{cn} \end{bmatrix} + \begin{bmatrix} V_{nN} \\ V_{nN} \\ V_{nN} \end{bmatrix} \quad (\text{I.16})$$

where V_{nN} is the voltage difference between the star point n of the load and the negative rail of the DC bus N , called the 'Common Mode Voltage'. v_{an}, v_{bn}, v_{cn} are phase to-neutral voltages further simplification yields the following expressions of a three-phase inverter model:

$$\begin{bmatrix} V_{an} \\ V_{bn} \\ V_{cn} \end{bmatrix} = \frac{V_{dc}}{3} \begin{bmatrix} 2 & -1 & -1 \\ -1 & 2 & -1 \\ -1 & -1 & 2 \end{bmatrix} \begin{bmatrix} S_A \\ S_B \\ S_C \end{bmatrix} \quad (I.17)$$

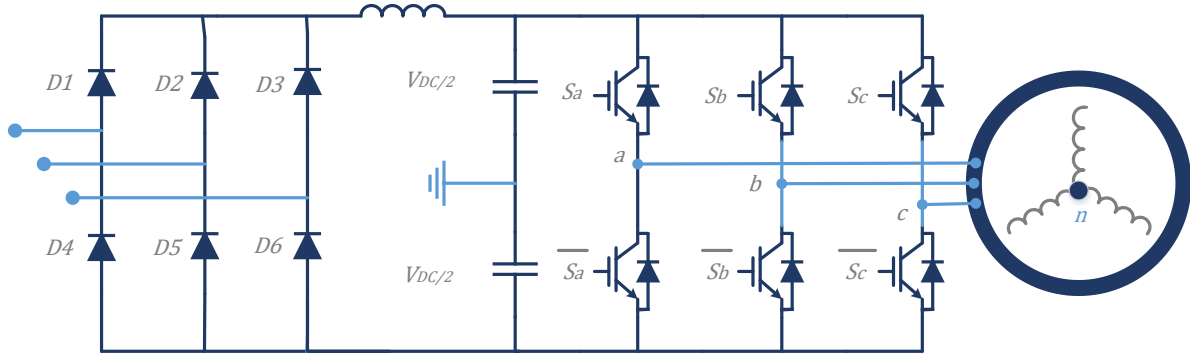


Figure I.4. Three phase inverter (six switches).

In addition, any three-phase system (defined by: $V_{An}(t), V_{Bn}(t), V_{Cn}(t)$) can be represented uniquely by a rotating vector \vec{V}_S :

$$\vec{V}_S = \frac{2}{3} [V_{An} + V_{Bn}e^{j2\pi/3} + V_{Cn}e^{j4\pi/3}] \quad (I.18)$$

Since the operation of the higher and lower switches are complimentary. The total possible outputs are $(2^3) = 8$ (000, 001, 010, 011, 100, 101, 110, 111). Here 0 indicates the switch is ‘OFF’ and 1 represents the switch is ‘ON’. Thus, there are six active switching states and two zero switching states. The space vectors are shown graphically in complex plan $\alpha\beta$ in Figure I.5.

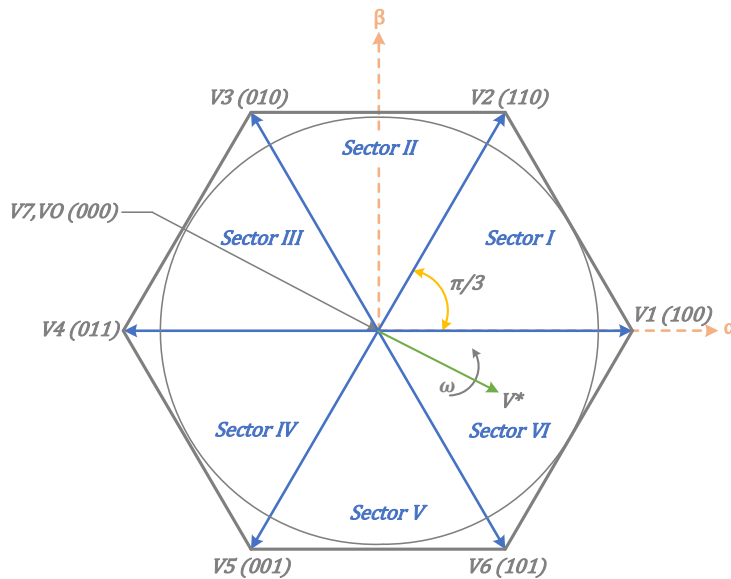


Figure I.5. Different voltage vectors generated by a six-switch inverter.

I.3.2. NINE-SWITCH VOLTAGE SOURCE INVERTER

The classical dual-output inverter consists of two separate two-level inverters connected in parallel. This topology has been used extensively in the industry, especially when independent control of two motors is required. The nine-switch inverter (NSI), as its name infers, has three less switches as compared to the classical dual output inverter. It has been conceived by replacing the middle six switches of the classical dual output inverter by only three switches, both inverters are shown in Figure I.6.

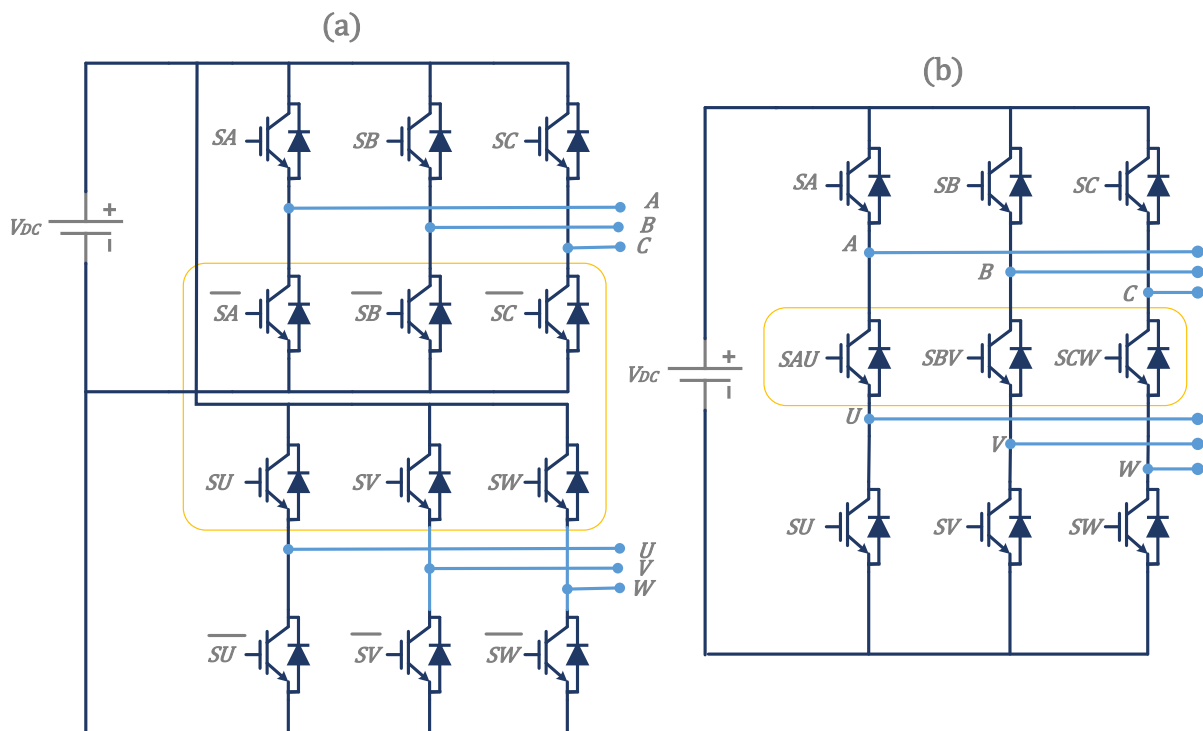











Figure I.6. (a) The classical Dual output inverter, (b) nine-switch inverter.

In order to avoid closing the three switches of the same leg simultaneously and therefore shorting the DC source, a XOR logic gate whose inputs are the two gate signals of the upper and lower switches generates the gate signal of the middle switch.

The NSI can be viewed as two conventional two-level inverters sharing the middle three switches. It is composed of three legs and each leg contains three switches. In each of the three legs and at any given instant, only one switch out of the three is allowed to be open in order to avoid short-circuiting the power supply through the inverter legs and to avoid keeping the loads floating. Consequently, the NSI has 27 (3^3) possible switching combinations.

Each leg can be in three different switch ON-OFF position. These positions are referred as $\{1\}$, $\{0\}$, and $\{-1\}$, as is illustrated in Table I.1.

Table I.1. NSI legs states.

Leg state Switch position	0	1	-1
<i>SJU</i>	OFF 	ON 	ON 
<i>SJM</i>	ON 	OFF 	ON 
<i>SJL</i>	ON 	ON 	OFF 

Referring to Table I.1 and Table I.2 shows all permissible states of the three legs. Due to the aforementioned constraint, only 27 states are allowed and it can be classified in 5 groups [5]:

- **Zero vectors:** Both outputs are in zero state. In zero state, a load is short-circuited through one of the DC rails.
- **Upper active vectors:** Upper output is in active state but lower output is in zero state.
- **Lower active vectors:** Lower output is in active state but upper output is in zero state.
- **Same active vectors:** Both outputs are in similar active state.
- **Middle active vectors:** Outputs are in different active states (neighbor active states).

These NSI states are also denoted as $V_x V_y$ where V_x refers to the voltage space vector of the upper ‘sub-inverter’ whereas V_y refers to the voltage space vector of the lower ‘sub-inverter’, referring to the 27 switching combinations we can notice that the NSI has two modes of operation. Mode 1, where loads can be supplied simultaneously for only a limited number of vectors (Same Active vectors and Middle active vectors). In mode2, loads of the NSI can be driven in alternate manner either for all possible combinations or only for the remaining switching combinations from mode 1. It should be noted that in the alternate supply by the NSI (i.e., mode2), when one load is in active state (i.e., supplied by the NSI) the second load is in zero state (i.e., its three terminals are shorted to one of the DC rails.) and vice versa. The sum of modulation indices of the two ‘sub-inverters’ can reach up to 1.15. On the other hand, when loads of the NSI are supplied simultaneously, the middle switches are all ON (i.e., closed) and therefore the NSI behaves as an ordinary two-level inverter supplying two loads in parallel. In this case, modulation indices of each of the two loads can be reach up to 1.15 in addition if two

Y-connected loads are to be driven by the NSI, the peak fundamental phase voltage of each load is given as follows [5] :

$$V_{an_{Peak(i)}} = m_i \cdot V_{in} / 2 \quad (I.18)$$

Table I.2. NSI leg states and their corresponding Voltage space vectors $V_x V_y$.

$V_x V_y$	Leg A	Leg B	Leg C	Type
$V_7 V_0$	1	1	1	Zero vectors
$V_7 V_7$	0	0	0	
$V_0 V_0$	-1	-1	-1	
$V_1 V_0$	1	0	0	Upper active vectors
$V_2 V_0$	1	1	0	
$V_3 V_0$	0	1	0	
$V_4 V_0$	0	1	1	
$V_5 V_0$	0	0	1	
$V_6 V_0$	1	0	1	
$V_7 V_1$	-1	1	1	
$V_7 V_2$	-1	-1	1	
$V_7 V_3$	1	-1	1	
$V_7 V_4$	1	-1	-1	
$V_7 V_5$	1	1	-1	
$V_7 V_6$	-1	1	-1	
$V_1 V_1$	-1	0	0	Same active vectors
$V_2 V_2$	-1	-1	0	
$V_3 V_3$	0	-1	0	
$V_4 V_4$	0	-1	-1	
$V_5 V_5$	0	0	-1	
$V_6 V_6$	-1	0	-1	
$V_2 V_1$	-1	1	0	Middle active vectors
$V_2 V_3$	1	-1	0	
$V_4 V_3$	0	-1	1	
$V_4 V_5$	0	1	-1	
$V_6 V_5$	1	0	-1	
$V_6 V_1$	-1	0	1	

I.4. BACKGROUND ON INDUCTION MOTOR DRIVES

Since the inception of AC machines, several techniques have evolved to control their speed, torque, and flux. The basic controlling parameters are the voltage and frequency of the applied voltage/current to the motor. Power electronic converters are used as an interface between the

grid supply and the electric motors. These power electronic converters, in most cases, are AC-DC-AC converters (more commonly called ‘inverters’) for AC machine drives.

The control of AC machines can be broadly classified into ‘scalar’ and ‘vector’ controls (Figure 1.7). Scalar controls are easy to implement and offer a relatively steady-state response, even though the dynamics are sluggish. To obtain high precision and good dynamics, as well as a steady-state response, ‘vector’ control approaches are to be employed with closed-loop feedback control. Thus, this work focuses on the ‘vector’ based approaches, namely Direct Torque Control.

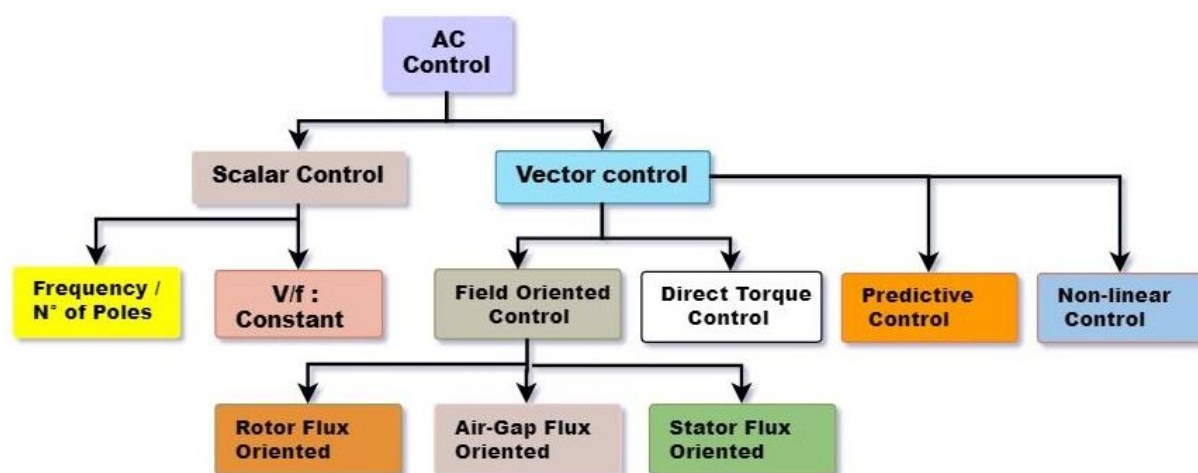


Figure I.7. AC motor control schemes.

I.5 CONCLUSION

In this chapter, we have presented the modelling process of the induction motor; the six-switch and the nine-switch voltage source inverters. Furthermore, a brief introduction to induction motor drives and a general classification of the control methods have been offered. The next chapter will be devoted to the study of the basic concepts of direct torque control ‘DTC’ used for driving the asynchronous induction motor.

Chapter II:

Direct Torque Control of Induction Motor

II.1 INTRODUCTION

Theoretical principles of direct torque control (DTC) for high performance drives were introduced in the second half of the 1980s [6]. Compared with field-oriented control, with origins that date back to the beginning of the 1970s, DTC is a significantly newer concept. It took almost 20 years for vector control to gain acceptance by industry. In contrast, the concept of DTC has been taken on board by industry relatively quickly in only ten years [6]. The on-off control of converter switches is used for the decoupling of the non-linear structure of the induction machine [6]. The most frequently discussed and used power electronic converter in DTC drives is a voltage source inverter.

This chapter is mainly intended for the description of the direct torque control, where the principle of regulating the stator flux and the electromagnetic torque is explained as well as the procedure for estimating these two quantities. The speed regulation of the induction motor is also presented in this chapter.

II.2. PRINCIPAL OF DIRECT TORQUE CONTROL

The main idea of the DTC is to choose the best vector of voltage that drives the inverter and keeps flux and torque in allowing bandwidth with minimum ripple. The block diagram of the DTC scheme is shown in Figure II.1. The flux and torque estimations, which are performed by means of mathematical model of induction motor, are needed for DTC. The stator flux vector can be calculated using the measured current and voltage vectors. Torque is estimated as a cross product of estimated stator flux linkage vector and measured motor current vector. The estimated flux magnitude and torque are then compared with their respective desired values and the resulting values are fed into the two-level and three-level hysteresis comparators

respectively. The outputs of both stator flux and torque comparators together with the position of the stator flux are used as inputs of the switching table (see Table II.1). Which is used for the selection of an appropriate voltage vector. It is noteworthy that because of the rotor time constant is larger than the stator one, the rotor flux changes slowly compared to the stator flux; in fact, the rotor flux can be assumed constant. If it happens that there is a deviation from the reference more than the allowed tolerance band, the hysteresis controller and switching table help choose an appropriate inverter state to make flux and torque return to their tolerance band as quickly as possible [7].

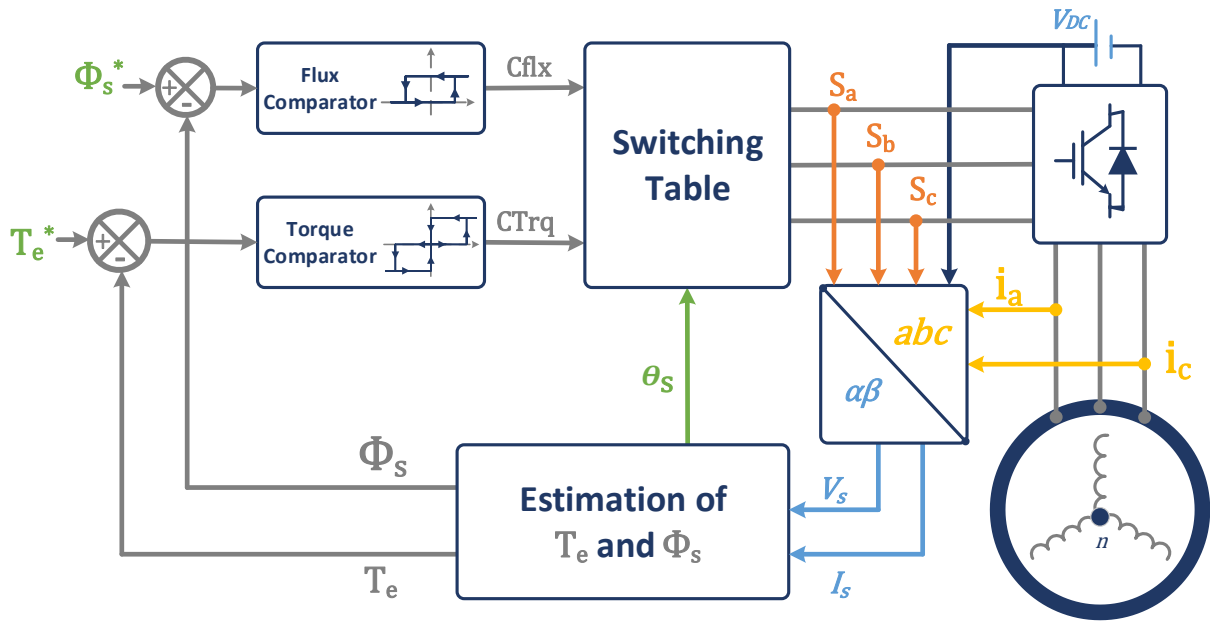


Figure II.1. Basic DTC bloc diagram.

II.3. CONTROL OF STATOR FLUX AND ELECTROMAGNETIC TORQUE

II.3.1. CONTROL OF STATOR FLUX

Basing on the induction motor model in stationary frame, the stator flux equation can be expressed as follows [8]:

$$\begin{cases} \phi_{s\alpha} = \int (v_{s\alpha} - R_s i_{s\alpha}) dt \\ \phi_{s\beta} = \int (v_{s\beta} - R_s i_{s\beta}) dt \end{cases} \quad (\text{II.1})$$

Considering that, the control of the switches of the inverter is done by control period (sampling) T_e and that at each of these periods the states S_a , S_b , and S_c are kept constant. The method of numerical integration of the rectangles makes it possible to obtain an expression of the sample $k + 1$ of the stator flux in the following form:

$$\begin{cases} \phi_{s\alpha}(k+1) = \phi_{s\alpha}(k) + [V_{s\alpha}(k) - R_s i_{s\alpha}(k)] T_e \\ \phi_{s\beta}(k+1) = \phi_{s\beta}(k) + [V_{s\beta}(k) - R_s i_{s\beta}(k)] T_e \end{cases} \quad (\text{II.2})$$

A vector inscription of this expression can be given by:

$$\vec{\phi}_s(k+1) = \vec{\phi}_s(k) + [\vec{V}_s(k) - R_s \vec{I}_s(k)] T_e \quad (\text{II.3})$$

We can neglect the stator resistance voltage drop compared to \vec{V}_s for high-speed regions. Then equation (II.3) can be written as:

$$\vec{\phi}_s(k+1) = \vec{\phi}_s(k) + [\vec{V}_s(k)] T_e \quad (\text{II.4})$$

Equation (II.4) means that the stator flux can be changed by the application of stator voltage during a time k . The stator flux vector's extremity moves in direction given by the voltage vector and making a circular trajectory (Figure II.2).

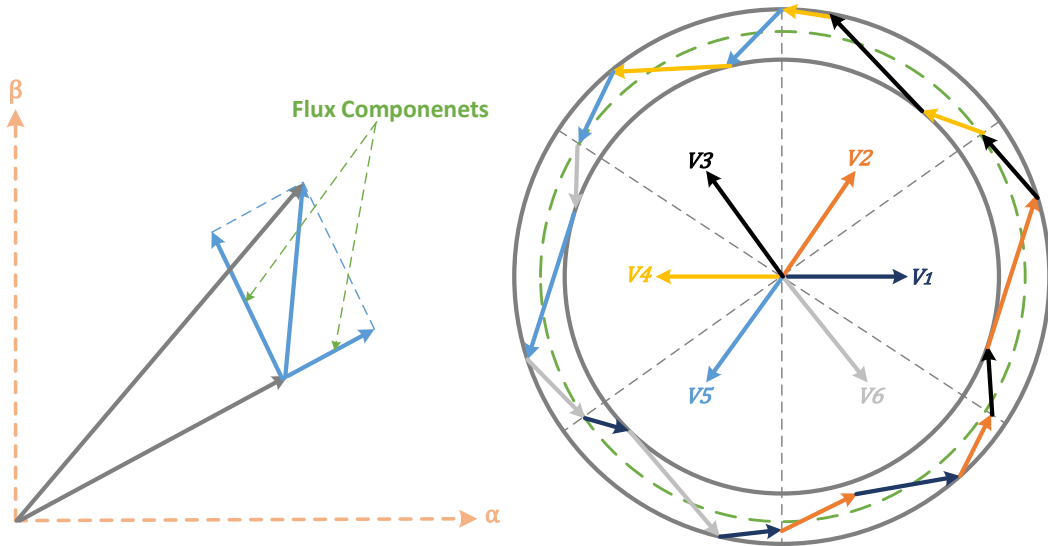


Figure II.2. Evolution of stator flux vector in the complex plan.

A two-level hysteresis comparator is used for flux regulation. It allows dropping easily the flux vector extremity within the limits of the two concentric circles with close radius. The choice of the hysteresis bandwidth depends on the switching frequency of the inverter Figures II.2 and II.3.

$$\begin{aligned} Cflx &= 1 \text{ if } \Delta \phi_s > h_{\phi_s} \\ Cflx &= 0 \text{ if } \Delta \phi_s \leq -h_{\phi_s} \end{aligned} \quad (\text{II.5})$$

where h_{ϕ_s} is hysteresis band of stator flux.

The stator flux error is defined by the difference between the reference value of flux $|\phi_s^*|$ and the actual estimated value $|\phi_s|$:

$$\Delta\phi_s = |\phi_s^*| - |\phi_s| \quad (\text{II.6})$$

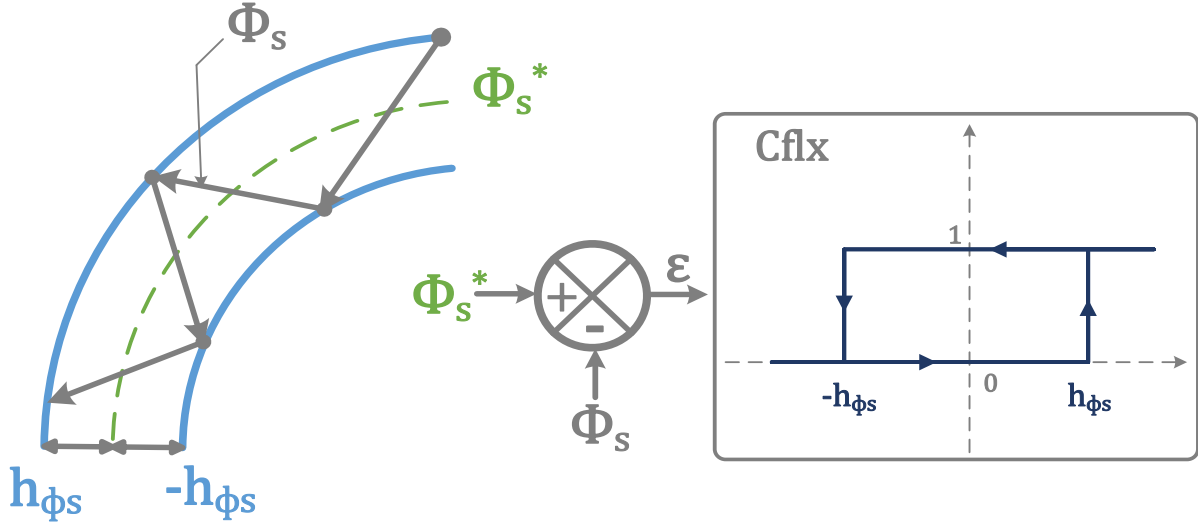


Figure II.3. Two-level hysteresis comparator for stator flux control.

II.3.2. CONTROL OF ELECTROMAGNETIC TORQUE

By eliminating i_s from equation (I.2), one can obtain:

$$\vec{I}_r = \frac{1}{\sigma} \left(\frac{\vec{\phi}_r}{L_r} - \frac{L_m}{L_r L_s} \vec{\phi}_s \right) \quad (\text{II.7})$$

It can be proven in the steady state, the rotor and stator flux vectors are linked by the following relation in the steady state:

$$\vec{\phi}_r = \frac{L_m}{L_s} \frac{1}{1 + j\sigma\omega T_r} \vec{\phi}_s \quad (\text{II.8})$$

Substituting Equation (II.7) into (I.7) from chapter one, the general expression of electromagnetic torque is given by :

$$T_e = p \frac{L_m}{\sigma L_r L_s} \vec{\phi}_s \times \vec{\phi}_r = p \frac{L_m}{\sigma L_r L_s} |\phi_s| |\phi_r| \sin \theta_{sr} \quad (\text{II.9})$$

where \times stands for scalar product, θ_{sr} angle between the stator and rotor flux vectors and

$\sigma = 1 - \frac{L_m^2}{L_r L_s}$ is the total leakage coefficient of the IM.

From expression (II.9), it is clear that the electromagnetic torque is controlled by the stator and rotor flux amplitudes. If these quantities are maintained constant, the torque can be

controlled by only adjusting the load angle θ_{sr} . The torque regulation can be realized using three-level hysteresis comparator (see Figure II.4). The logical output $Ctrq$ of the torque controller is defined as:

$$\begin{aligned} Ctrq &= 1 & \text{if } \Delta T_e > h_{T_e} \\ Ctrq &= 1 & \text{if } -h_{T_e} \leq \Delta T_e \leq h_{T_e} \\ Ctrq &= 0 & \text{if } \Delta T_e < -h_{T_e} \end{aligned} \quad (\text{II.10})$$

where h_{T_e} is hysteresis band of torque, on the other hand torque error is defined by the difference between the reference value of the torque T_e^* and the actual estimated value T_e :

$$\Delta T_e = T_e^* - T_e \quad (\text{II.11})$$

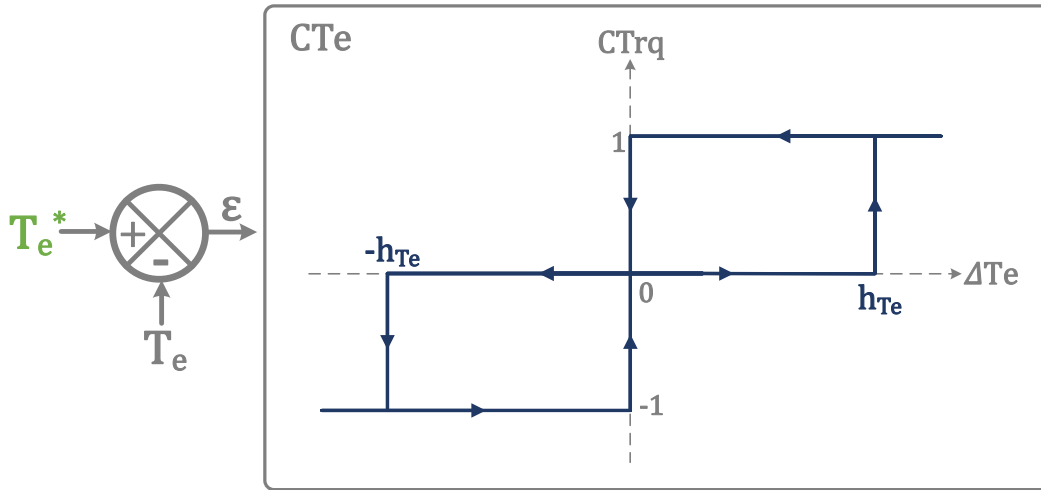


Figure II.4. Three-level hysteresis comparator for electromagnetic torque control.

II.4. ESTIMATION OF STATOR FLUX AND ELECTROMAGNETIC TORQUE

II.4.1. STATOR FLUX ESTIMATION

The vector flux is estimated using equation (II.1), which requires knowledge of the components of the stator current vector $i_{s\alpha}$ and $i_{s\beta}$ and that of the vector stator voltage $v_{s\alpha}$ and $v_{s\beta}$. The stator voltage components $v_{s\alpha}$ and $v_{s\beta}$ are obtained by applying Concordia transformation on the output voltage of the three-phase VSI and the switching signals (S_A, S_B, S_C) which are given by:

$$\begin{cases} v_{s\alpha} = \sqrt{\frac{2}{3}} V_{DC} \left[S_A - \frac{1}{2}(S_B + S_C) \right] \\ v_{s\beta} = \sqrt{\frac{1}{2}} V_{DC} (S_B - S_C) \end{cases} \quad (\text{II.12})$$

The stator currents components $i_{s\alpha}$ and $i_{s\beta}$ can be obtained also by applying Concordia transformation on the measured currents (I_{sB}, I_{sB}, I_{sC}):

$$\begin{cases} i_{s\alpha} = \sqrt{\frac{2}{3}}i_{sA} \\ i_{s\beta} = \sqrt{\frac{1}{2}}(i_{sB} - i_{sC}) \end{cases} \quad (\text{II.13})$$

where $i_{sC} = -(i_{sB} + i_{sC})$ and $I_s = i_{s\alpha} + j i_{s\beta}$.

The amplitude of the stator flux is estimated from its two-phase components $\phi_{s\alpha}$ and $\phi_{s\beta}$:

$$\phi_s = \sqrt{\phi_{s\alpha}^2 + \phi_{s\beta}^2} \quad (\text{II.14})$$

The exact position of the stator flux space vector is not needed in DTC induction motor drives. It is only necessary to know in which sector (out of six possible ones) of the complex plane the vector is located. This can be done by deduction of the angle θ_s made by the flux vector with the stator frame of reference and is calculated as follows:

$$\theta_s = \tan^{-1} \frac{\phi_{s\beta}}{\phi_{s\alpha}} \quad (\text{II.15})$$

II.4.2. ELECTROMAGNETIC TORQUE ESTIMATION

The produced electromagnetic torque of the induction motor can be determined by the use of stator quantities (i.e., stator flux and stator currents). The torque formula is expressed as follows:

$$T_e = p(\phi_{s\alpha}i_{s\beta} - \phi_{s\beta}i_{s\alpha}) \quad (\text{II.16})$$

II.5. SWITCHING TABLE CONSTRUCTION

To maintain a decoupled control, a pair of hysteresis comparators receives the stator flux and torque errors as inputs. Then, the comparators outputs determine the appropriate voltage vector selection. However, the choice of voltage vector is not only depending on the output of hysteresis controllers but on the position of stator flux vector also. Thus, the circular stator flux vector trajectory will be divided into six symmetrical sectors (Table II.1). For each sector, the vectors (V_i and V_{i+3}) are not considered because both of them can increase or decrease the torque in the same sector according to the position of flux vector on the first or the second sector. If the zero vectors V_0 and V_7 are selected, the stator flux will stop moving, its magnitude will not change, and the electromagnetic torque will decrease, but not as much as when the

active voltage vectors are selected. The resulting look-up table for DTC, which was proposed by Takahashi, is presented in Table II.2. [8].

Table II.1. Generalized switching table.

	<i>Increases</i>	<i>Decreases</i>
ϕ_s	V_{i-1} and V_{i+1}	V_{i+2} and V_{i-2}
T_e	V_{i+1} and V_{i+2}	V_{i-1} and V_{i-2}

Table II. 2. Optimum voltage vector look-up table.

Flux	Torque	Sector 1	Sector 2	Sector 3	Sector 4	Sector 5	Sector 6
Cflx = 1	CTrq = 1	V ₂	V ₃	V ₄	V ₅	V ₆	V ₁
	CTrq = 0	V ₇	V ₀	V ₇	V ₀	V ₇	V ₀
	CTrq = -1	V ₆	V ₁	V ₂	V ₃	V ₄	V ₅
Cflx = 0	CTrq = 1	V ₃	V ₄	V ₅	V ₆	V ₁	V ₂
	CTrq = 0	V ₀	V ₇	V ₀	V ₇	V ₀	V ₇
	CTrq = -1	V ₅	V ₆	V ₁	V ₂	V ₃	V ₄

Active voltage vectors : 1 (100), 2 (110), 3 (010), 4 (011), 5 (001), 6 (101).

Zero voltage vectors: 7 (111), 0 (000).

II.6. SPEED REGULATION

The proportional-integral (PI) controller is used for the speed regulation. It is performed by comparing the speed reference signal to the actual measured speed value. Then the comparison error becomes the input of the PI controller. The pole placement method is used to determine the controller gains. A PI controller with anti-wind up is used as a speed controller for better performance of speed responses (lower overshoot, faster time response, reduced or zero steady state-error), it does so by canceling the windup phenomenon, which is caused by the saturation of the pure integrator [8]. This strategy consists on the correction of the integral action based on the difference between the control signal and the saturation limit. The difference value is passed through a gain block (tracking time constant T_i) before arriving as feedback to the integrator. Figure II.5 shows the speed anti-windup PI controller diagram block.

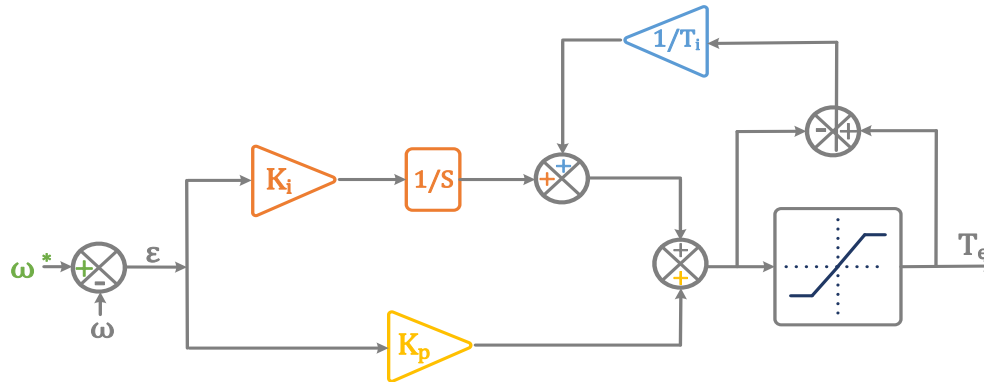


Figure II.5. Speed anti-windup PI controller.

II.7. SIMULATION RESULTS

To study the performance of the developed DTC model, a closed loop speed control of a 1.1KW induction motor (with characteristics given in the appendix) is simulated using Matlab/Simulink simulation package. Figure II.6 presents the developed simulation model.

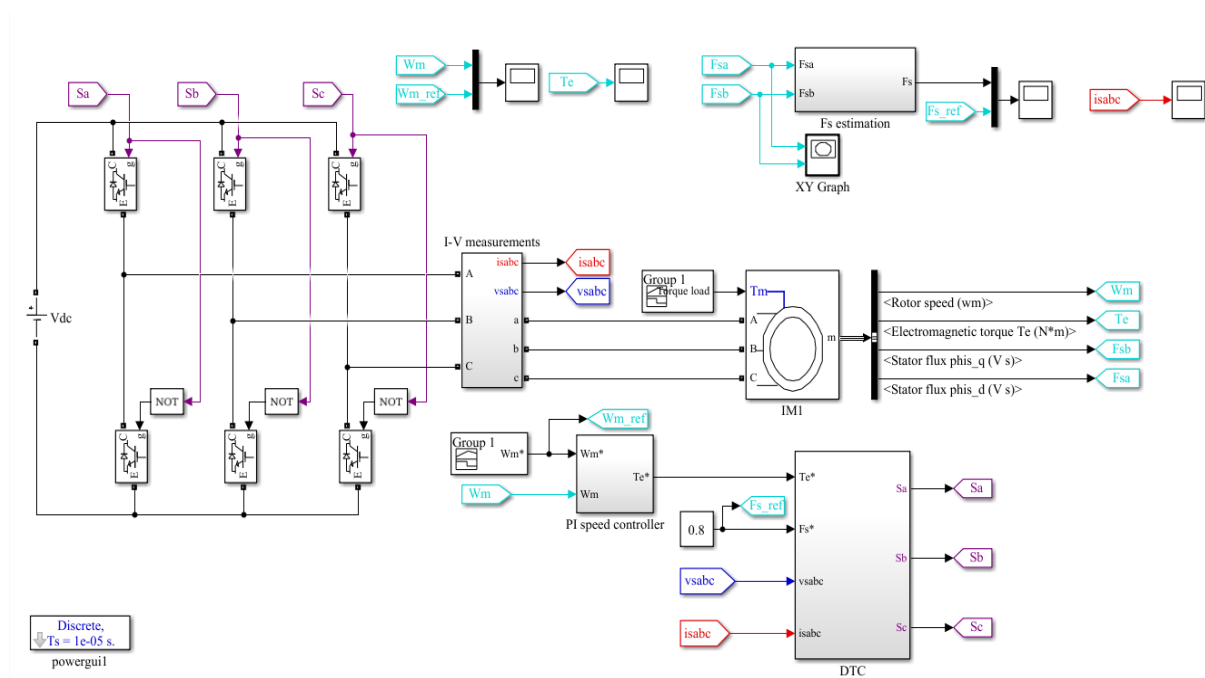


Figure II.6. Simulink block diagram of the developed DTC.

The simulation was carried out under the following conditions:

- The torque comparator hysteresis band is ± 0.1 Nm.
- The flux comparator hysteresis band is ± 0.01 Wb.
- The reference electromagnetic torque is recovered at the output of the PI controller.
- The reference flux is 0.8 Wb.
- The power sim induction motor model was used.
- A maximum step size of (0.01 ms).

❖ **Test 1: No-load start followed by load disturbances:**

The dynamic performance of developed DTC model is to be evaluated in this test; the later is conducted by maintaining a speed reference of ($\omega = 100$ Rad/s). The obtained results of the rotational speed, the electromagnetic torque, the stator flux, the stator currents and the stator flux trajectory respectively are shown in Figure II.7

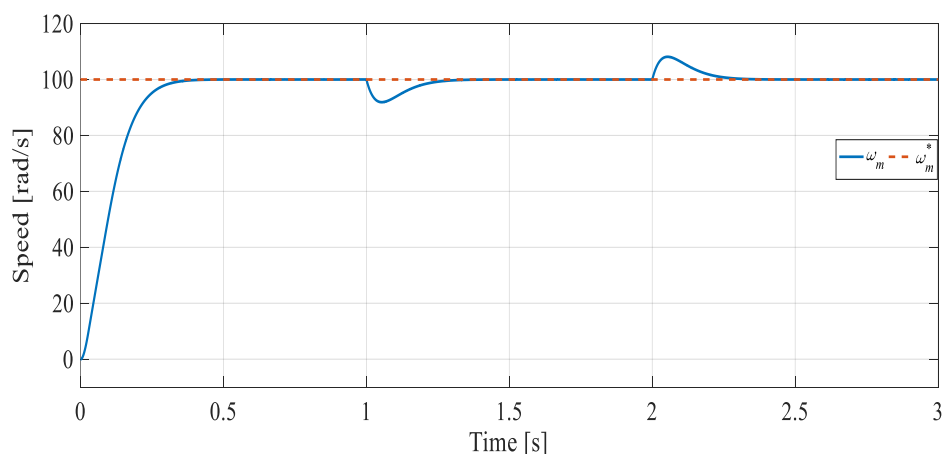
The test starts with no resistive load applied to IM; it can be noticed that the rotor speed judiciously follows its reference value with no steady state error nor overshoot and a rise time of (0.35s). The starting torque reaches a value of (7 Nm) and gradually decreases till it's approximately nullified; it is worth noting that both torque and rotor speed reach their expected values at the same time.

At ($t = 1$ s), a resistive torque load of (5 Nm) is applied to the motor; initially the speed drops but quickly recovers to its reference value, meanwhile the electromagnetic torque rapidly increases to reach its load target value of (5 Nm) with an over shoot of roughly (1 Nm).

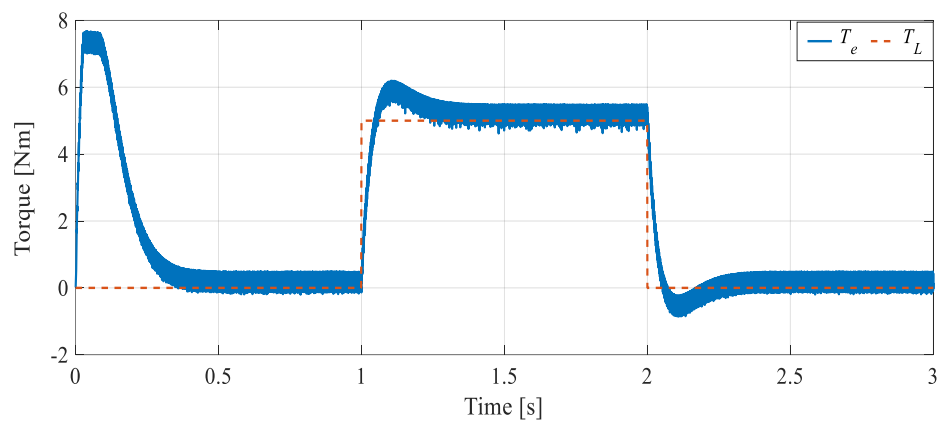
Suddenly, at ($t = 2$ s) the motor is unloaded, and the rotor speed rises but recovers afterwards and returns to (100 rad/s) while the electromagnetic torque underwent slightly before returning to nearly zero.

It can be observed that the stator current waveforms are sinusoidal in shape. The stator flux magnitude response has risen to its reference value of 8.0 Wb and was constrained within its hysteresis band of ± 0.01 Wb therefore; the flux trajectory draws the figure of a circle.

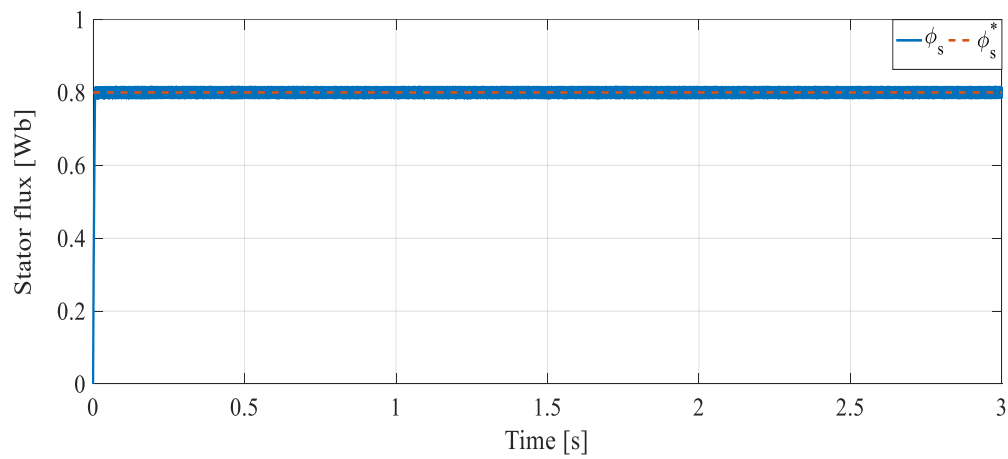
(a) Rotational speed



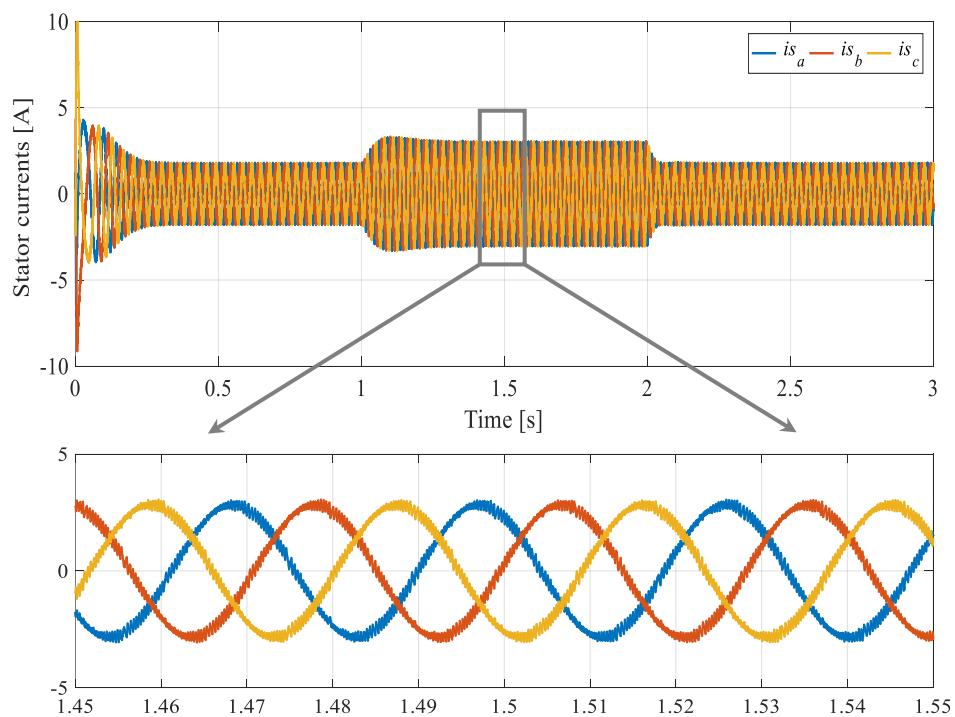
(b) Electromagnetic torque



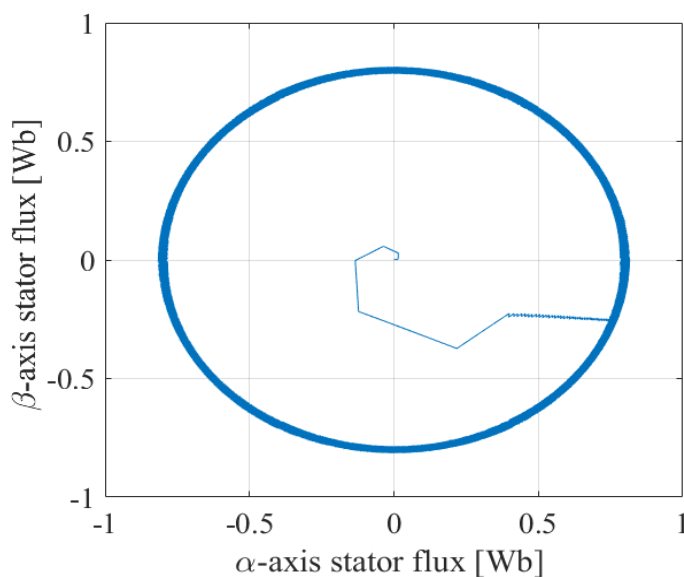
(c) Stator flux



(d) Stator current



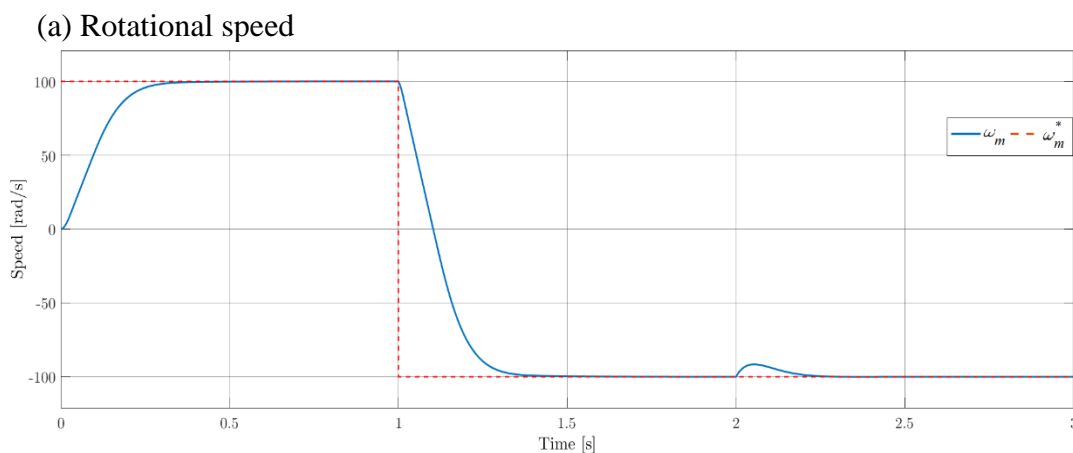
(e) Stator flux trajectory

**Figure II.7.** Simulation results of DTC for no-load start followed by load disturbances.

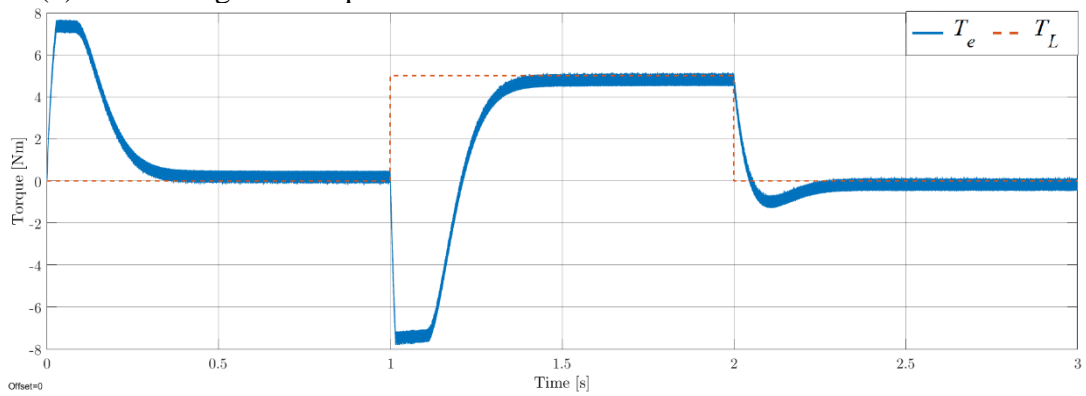
❖ **Test2: Reversed Rotation:**

This test was carried out in a similar fashion to the previous one, the only difference was the change of the reference speed from (100 Rad / s) to (-100 Rad / s) at (t = 1 sec), which was kept constant for the rest of the test duration, this negative reference value caused the reversal of rotation.

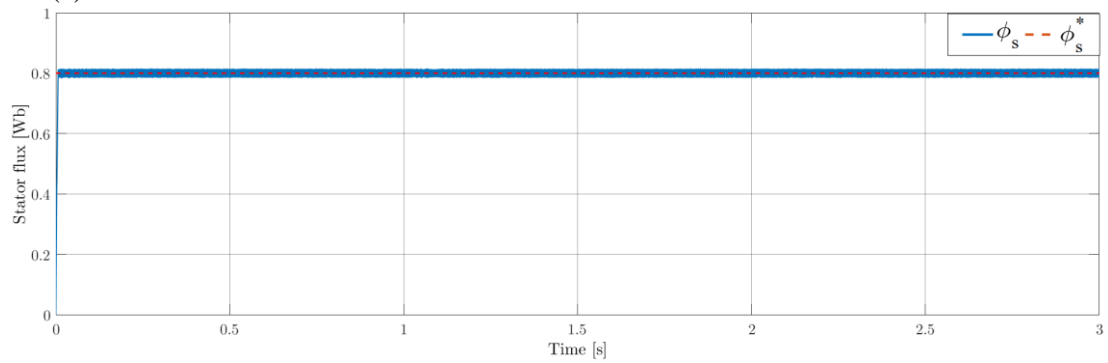
Figure II.8 shows the responses of the machine before and during the reversal of the direction of rotation. The simulation results show that there is a good follow-up to the newly applied reference speed of (-100 Rad/s) with no overshoot nor steady state error with good responses of both torque and flux.



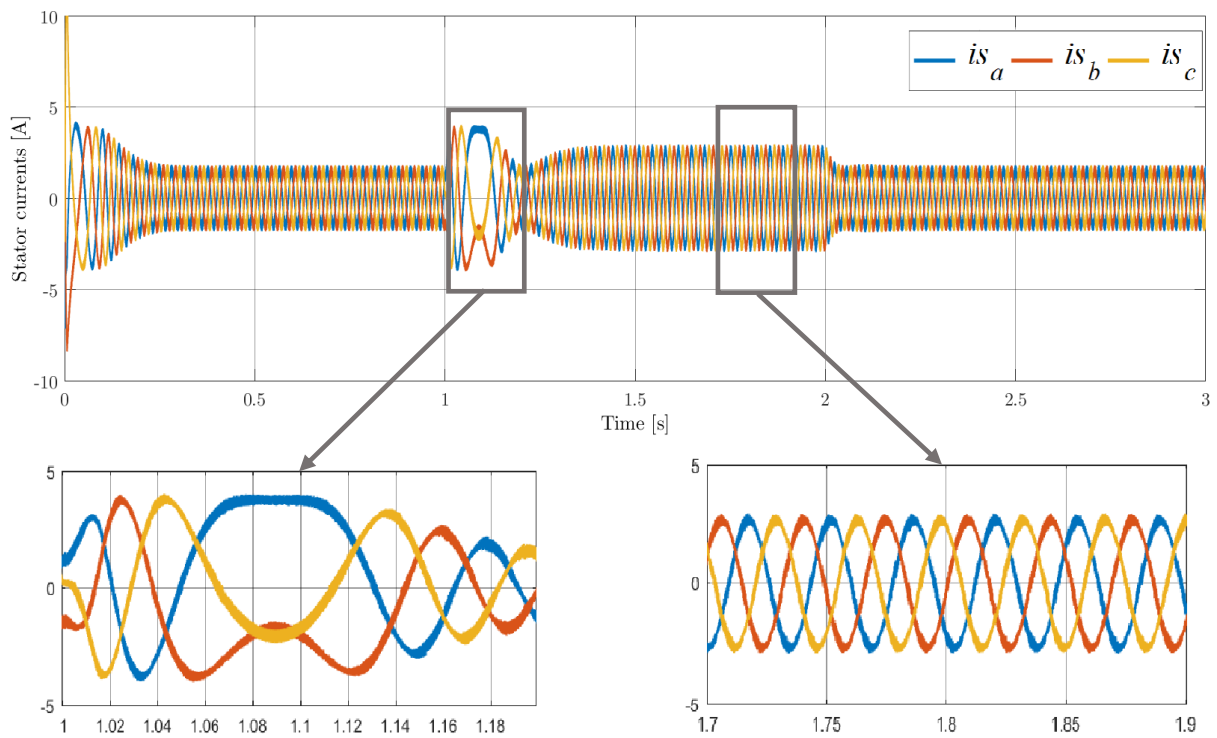
(b) Electromagnetic torque



(c) Stator flux



(d) Stator current



(e) Stator flux trajectory

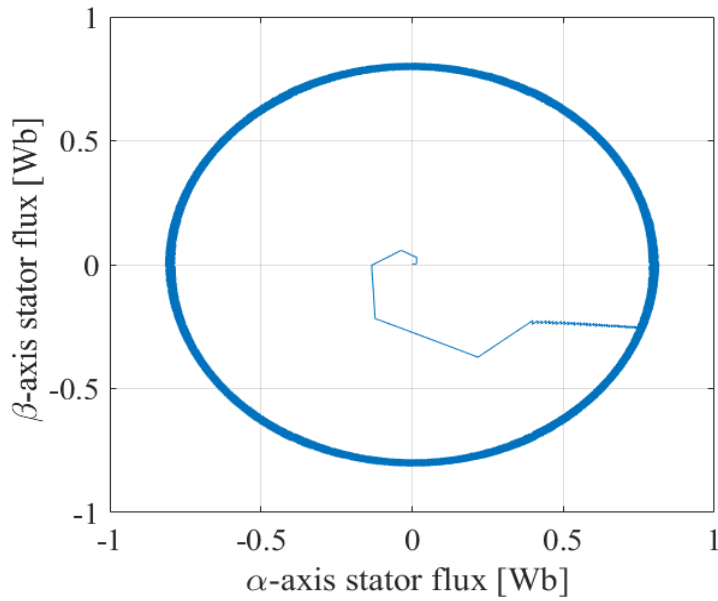


Figure II.8. Simulation results of DTC for reversed rotation.

II.8 CONCLUSION

This chapter explained the operation principles of direct torque control method, of which a scheme was presented detailing its function. The DTC method appears to be an efficient and simple way of controlling an induction machine. In order to test the performance of the control technique, numerical simulations were performed successfully followed by discussion and notes of the obtained results, which eventually concluded the good performance of the DTC method.

The next chapter will be devoted to the DTC technique of two IMs by the use of a nine-switch inverter.

Chapter III:

Direct Torque Control

of two Induction Motors

III.1. INTRODUCTION

Prior to the development of the nine-switch inverter (NSI), driving two three-phase loads independently, requires using a dual output inverter; this latter consists of two separate two-level inverters connected in parallel, which amounts to a system composed of twelve switches. Due to this high number of semi-conductor switches, several topologies, with less semi-conductor components counts, were presented as substitutes to this inverter, specifically, the B4 inverter [9] and the five-leg inverter (FLI) [10]. Recently, the NSI has been proposed in [11], this converter can be used to drive two three-phase loads independently. The main advantage of the NSI is that it has less switches than all its afore mentioned ancestors. Having the least number of semiconductor switches, the focus on exploiting the NSI in industrial applications has been noticeably higher [5]. On the other hand, thanks to the robustness of the direct torque control (DTC) scheme as compared to the other vector control schemes of induction motor (IM), the DTC is widely used in motion control of electric drives, especially for the switching table based direct torque control (ST-DTC) [12].

In order to exploit the powerful combination of the DTC control and the NSI in driving two IMs, this chapter suggests a DTC control scheme based on a synchronization algorithm, which basically, supply the two IMs simultaneously, whenever possible, otherwise it supplies the two loads in alternate manner.

III.2. STRUCTURE WITH TWO SIX-SWITCH VOLTAGE SOURCE INVERTERS

The topology of the dual two-level inverter (12-switch inverter) as shown in Figure III.1 consists of two individual two-level inverters (two Six-switch inverter). The two inverters are supplied by the same DC voltage source. This is processed by means of an arrangement of six legs, which in turns are composed by two power semiconductors in series. These last must operate in the complementary conduction mode to avoid short circuit of the dc-link. This six-phase voltage source inverter supplies dual three-phase induction motor with isolated neutrals.

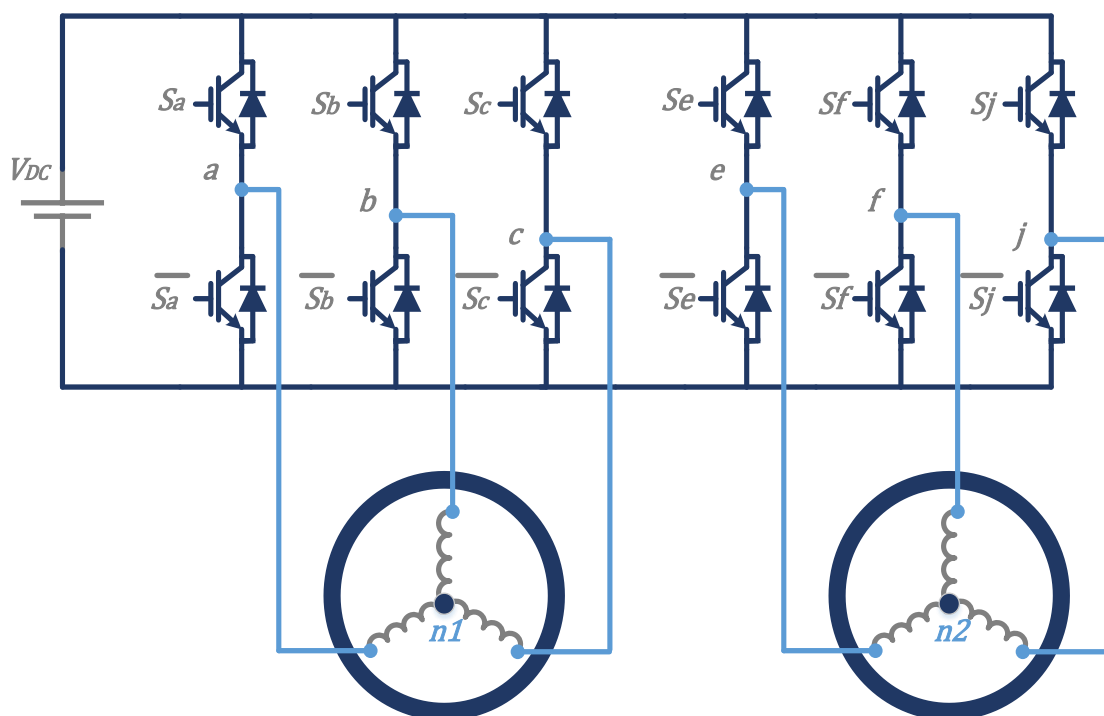


Figure III.1. Six-phase VSI connected to dual three-phase IM.

III.2.1. CONTROL SCHEME

The DTC basic scheme for dual-three-phase induction motor drives is shown in Figure III.2. Both induction motors are independently driven based on the estimated stator flux position for each IM separately; two different hysteresis controllers for torque and flux one for each induction motor are used to generate the inverter switching functions using two independent switching tables.

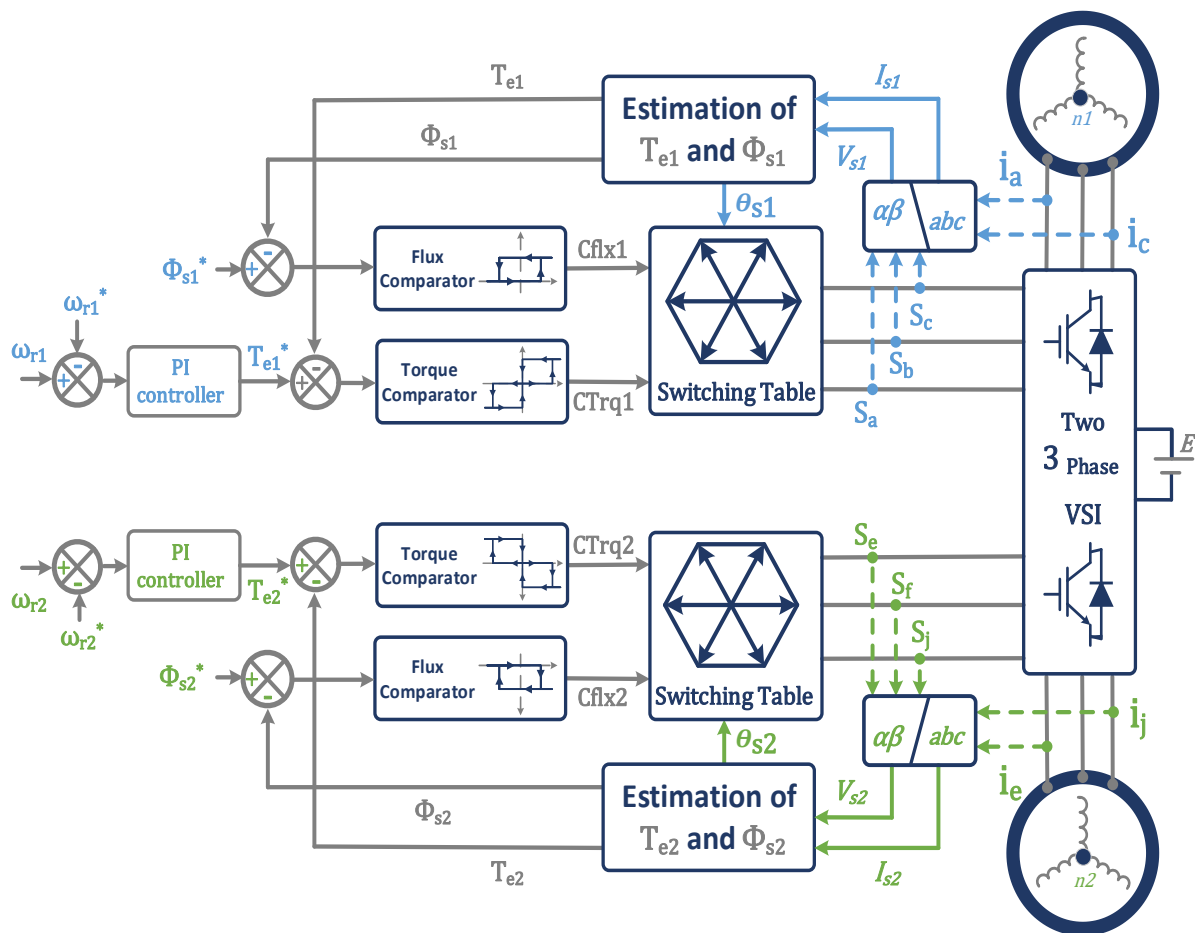


Figure III.2. DTC control scheme when applied six-phase VSI

III.2.2. SIMULATION RESULTS

In order to investigate the DTC with six-phase VSI, a simulation using the Simulink® software is carried out. Each individual DTC block was subjected to the same parameters used in chapter II, with two identical induction motors (with characteristics given in the appendix). Figure III.3 shows the simulink model of DTC block with six-phase VSI.

The motors are driven with several speed combinations. At each speed combination, a nominal load is coupled to each motor. The simulation results of both IMs are illustrated in Figure III.4.

- ❖ **For motor 01:** the test starts with a reference speed of (100 Rad/s) no load coupled with it. Then at ($t = 1s$) the reference speed is changed to (140 Rad/s) but the load torque is null, at ($t = 2s$) the reference speed is reduced to (80 Rad/s) and remains as such for the remainder of the test however the load torque won't be changed until ($t = 3s$) to a value of (5 Nm).

- ❖ **For motor 02:** For the duration of the entire test a nominal load torque of (3 Nm) was applied to the motor, however the reference speed will change from (100 Rad/s) at the start of test to reverse rotation with (-100 Rad/s) at ($t = 2$ s) and remains as such until the test concludes.

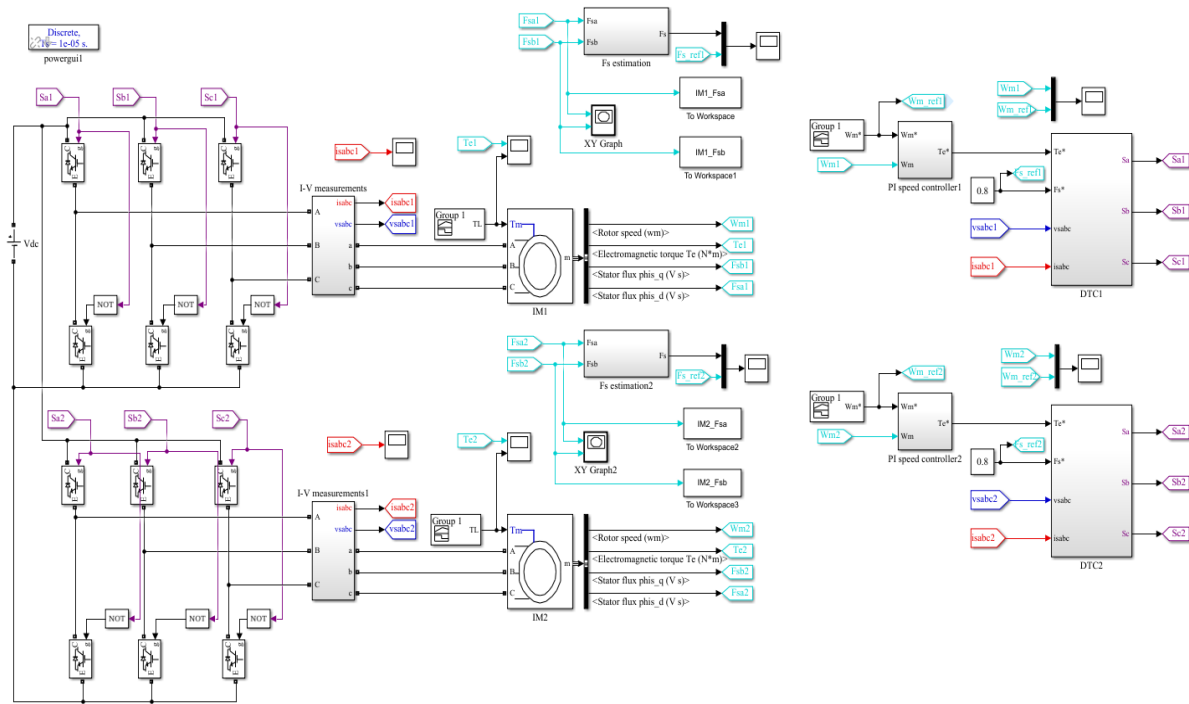


Figure III.3. Simulink model of DTC with six-phase VSI

Figure III.4(a) shows the simulation waveforms of the reference rotational speed (orange color), measured rotational speed (blue color for motor 1, green for motor 2); the system shows good speed responses for both machines with good tracking and short transient stage with no steady state error.

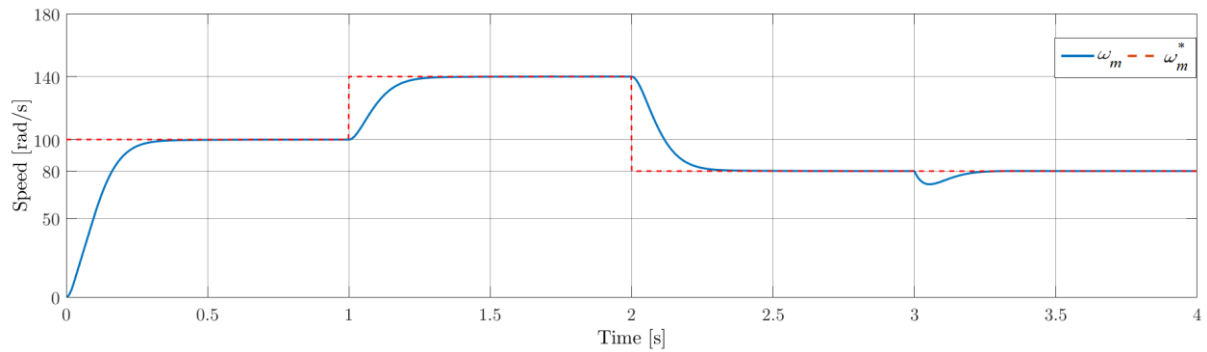
The evolution of electromagnetic torque for IM1 (blue color) and IM2 (green color) is shown in Figure III.4 (b). Again, both machines exhibit normal torque response for the DTC method, with a good follow up to the reference torque with in-range torque ripples.

Figure III.4 (d) shows the simulation transients of the stator phase currents for the induction motors 1 and 2. The results of simulation tests show that the stator phase current amplitudes depend on the operating and load state of the drive system and increase in dynamic states and reach a set value in the steady states.

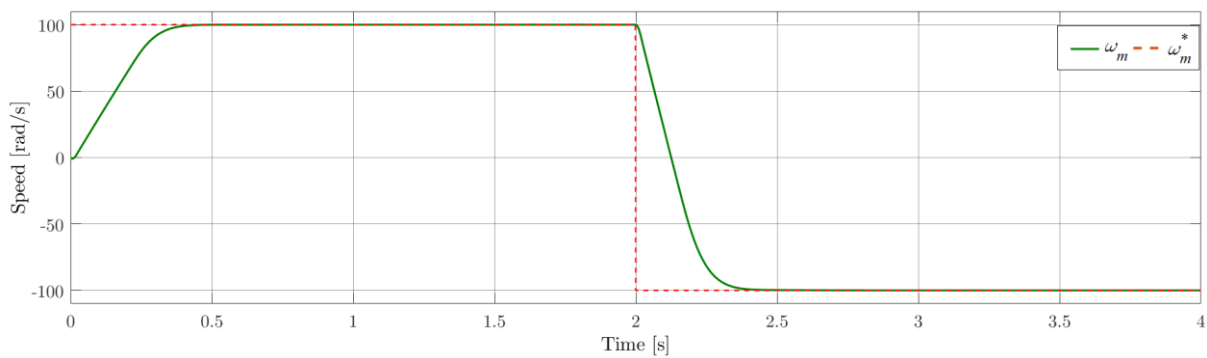
Figure III.4(c) illustrates the flux trajectory following its reference value with minor ripples that is translated into a circular shape in the flux locus of Figure III.4 (e).

(a) Rotational speed

IM1

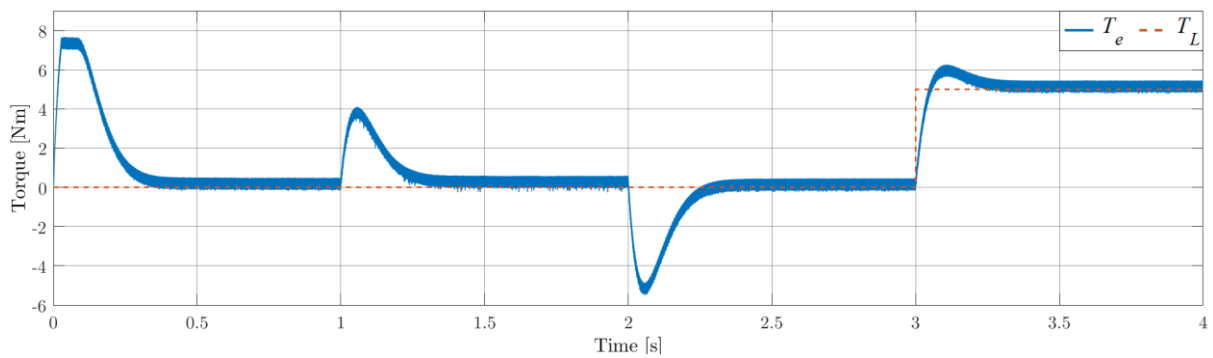


IM2

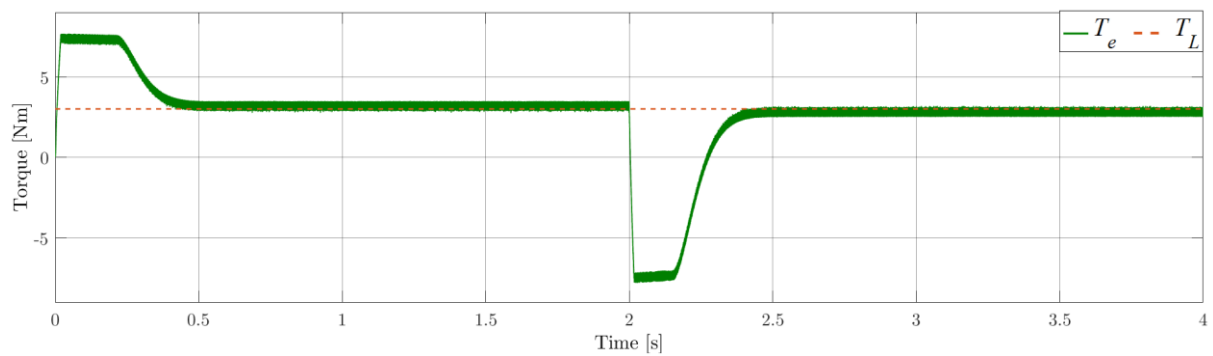


(b) Electromagnetic torque

IM1

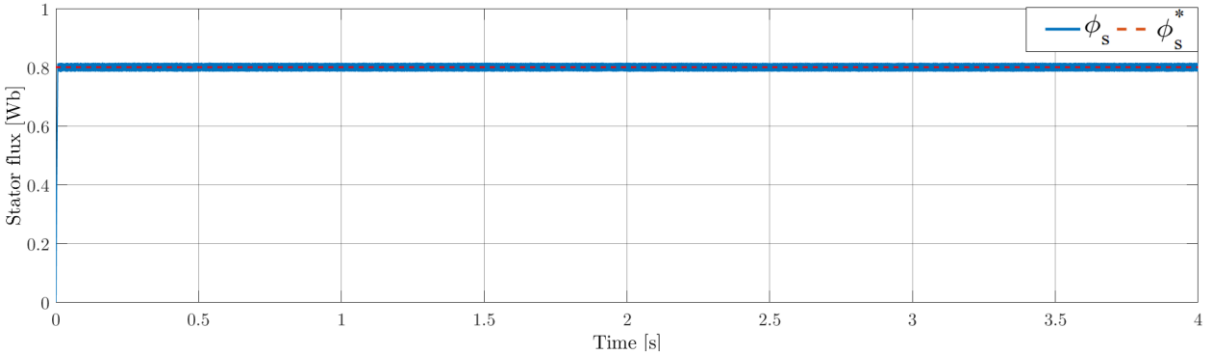


IM2

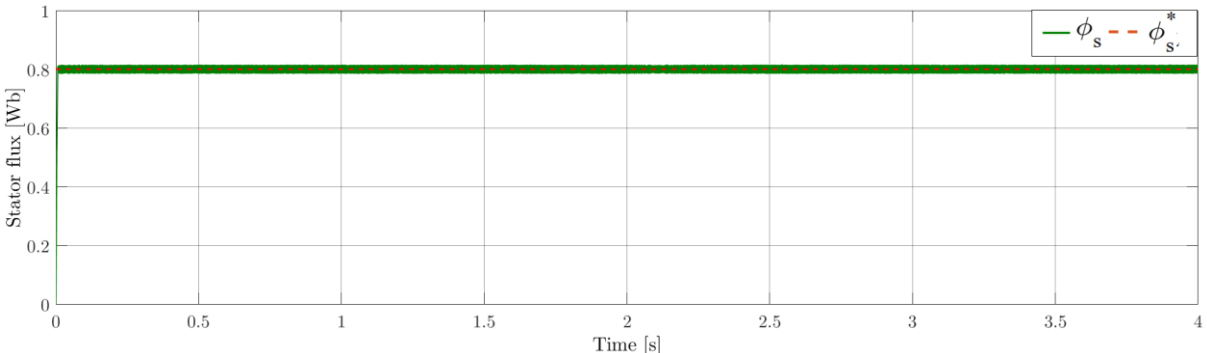


(c) Stator flux

IM1

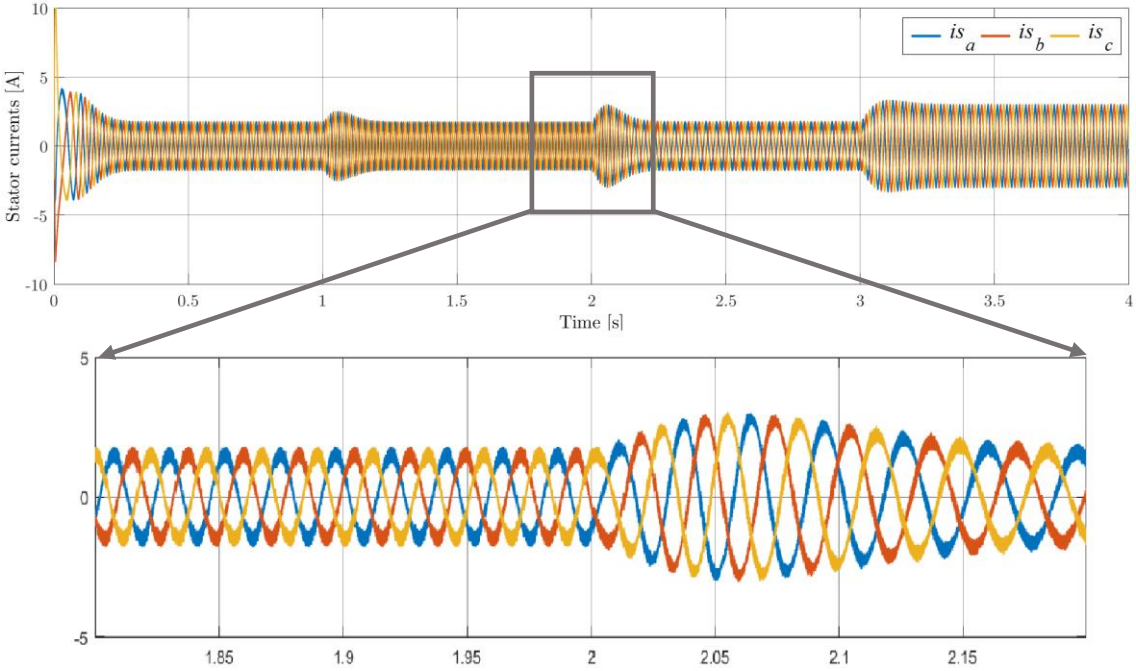


IM2

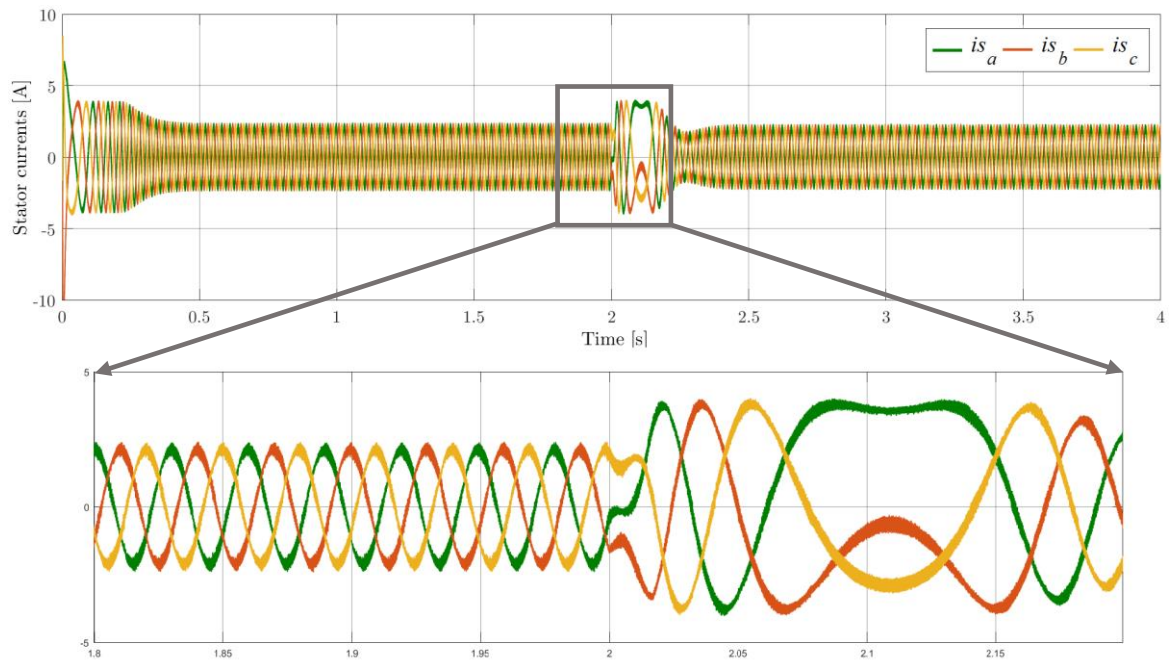


(d) Stator current

IM1



IM2



(e) Stator flux trajectory

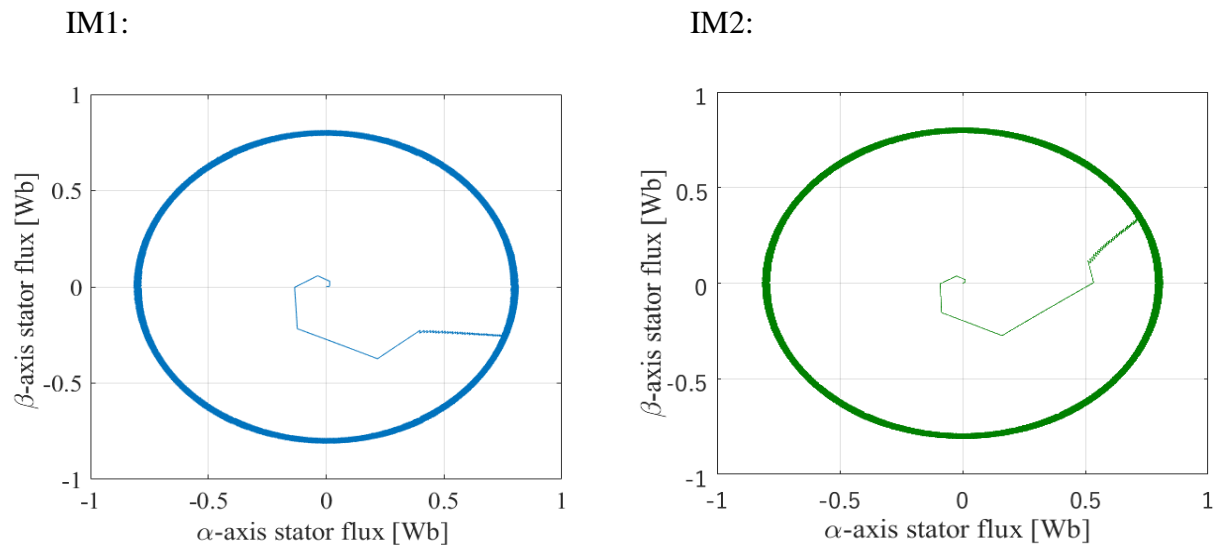


Figure III.4. Simulation results of DTC with six-phase VSI for several speed combinations coupled with nominal loads.

III.3. STRUCTURE WITH NINE-SWITCHES VOLTAGE SOURCE INVERTER

In case of applying the DTC to control the NSI, the generated inverter switching functions will not be supplied to the NSI directly, (see Figure III.5). A synchronization block is set to read these vectors to select the load that will be supplied next, based on an algorithm or automatically in an alternate manner.

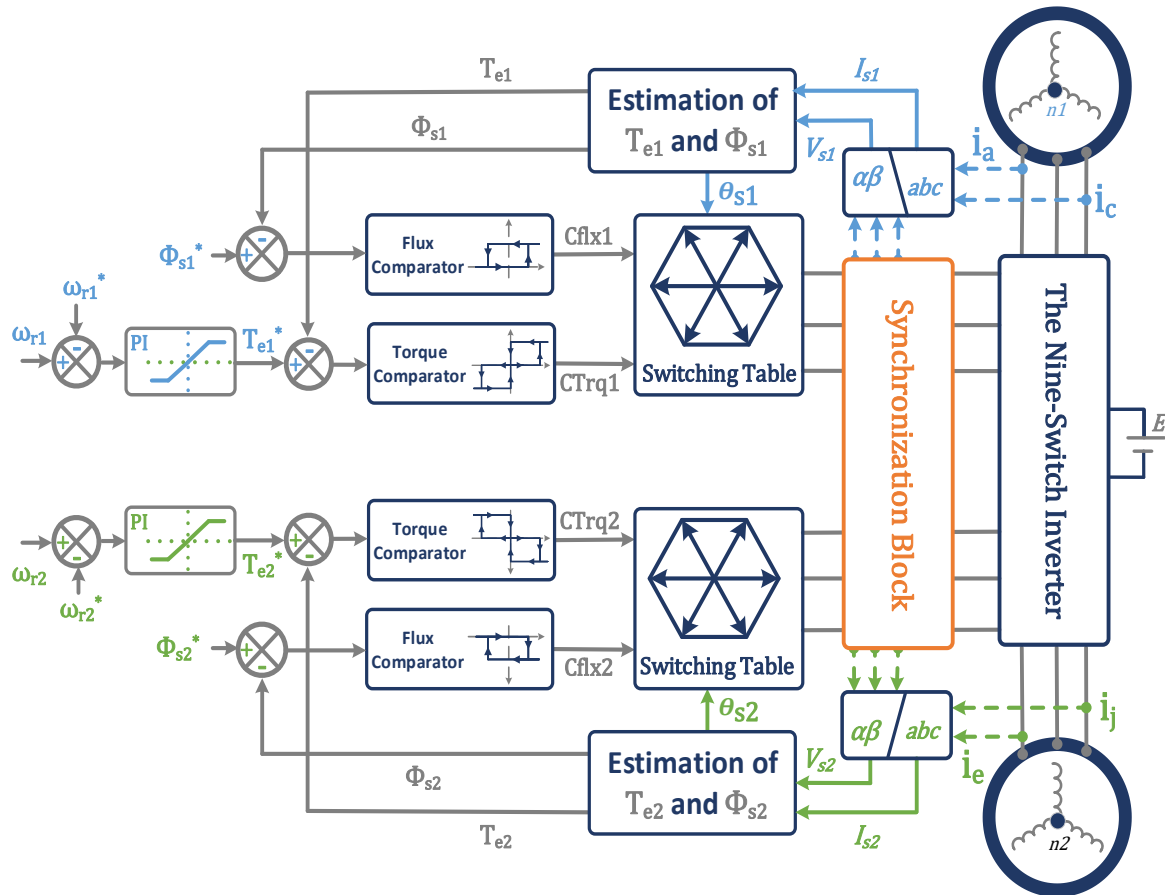


Figure III.5. Block diagram of DTC with NSI.

III.3.1. CONTROL SCHEME

In DTC control, the application of zero vector has little or no effect on motor's stator flux, but the rate of decrease of a motor's torque is directly proportional to the motor's speed of operation [5], leading to large torque ripples, especially if the motor in question is operating in high speed, eventually leading to mis-operation of the entire system. To mitigate the effect of significant dip in torque of any of the two motors and to avoid using a faster processing controller, which may erode the simplicity of the DTC control method, the presented algorithm will consider the inputs from the switching tables to ensure the simultaneous supply of the two motors. In the simultaneous drive of the two motors, faster response is obtained and the modulation indices can be increased to up to 1.15 each, which translate to high torque/speed capabilities [5]. (The flow chart of the suggested algorithm is demonstrated in Figure III.6)

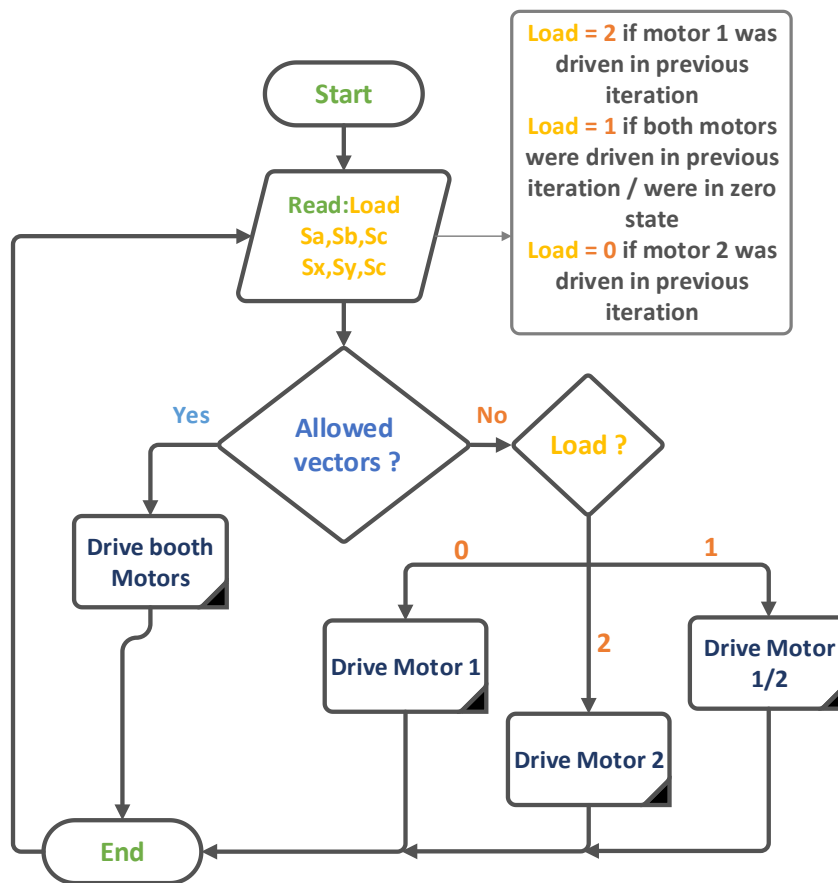


Figure III.6. Flowchart of the suggested algorithm.

According to Table I.2 and based on Figure III.7, the NSI can supply the two motors simultaneously, if the stator flux space vectors of these motors are in the same or neighboring sectors, this holds true for a longer time, when the motors are running at the same speed.

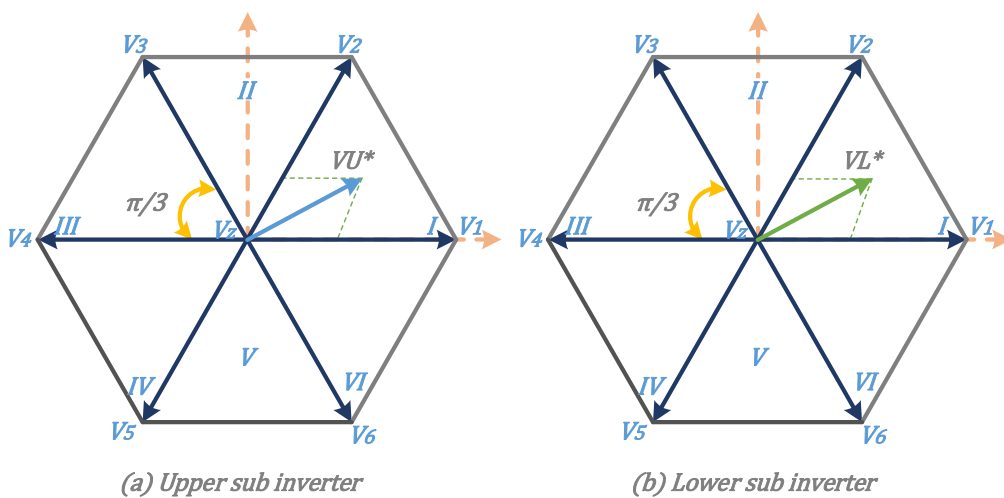


Figure III.7. Voltage space vector locations.

The proposed algorithm requires only the state vectors from the switching table as inputs to output the proper vectors for both ‘sub-inverters’ of the NSI. The Simulink model of synchronization block is illustrated in Figure III.8.

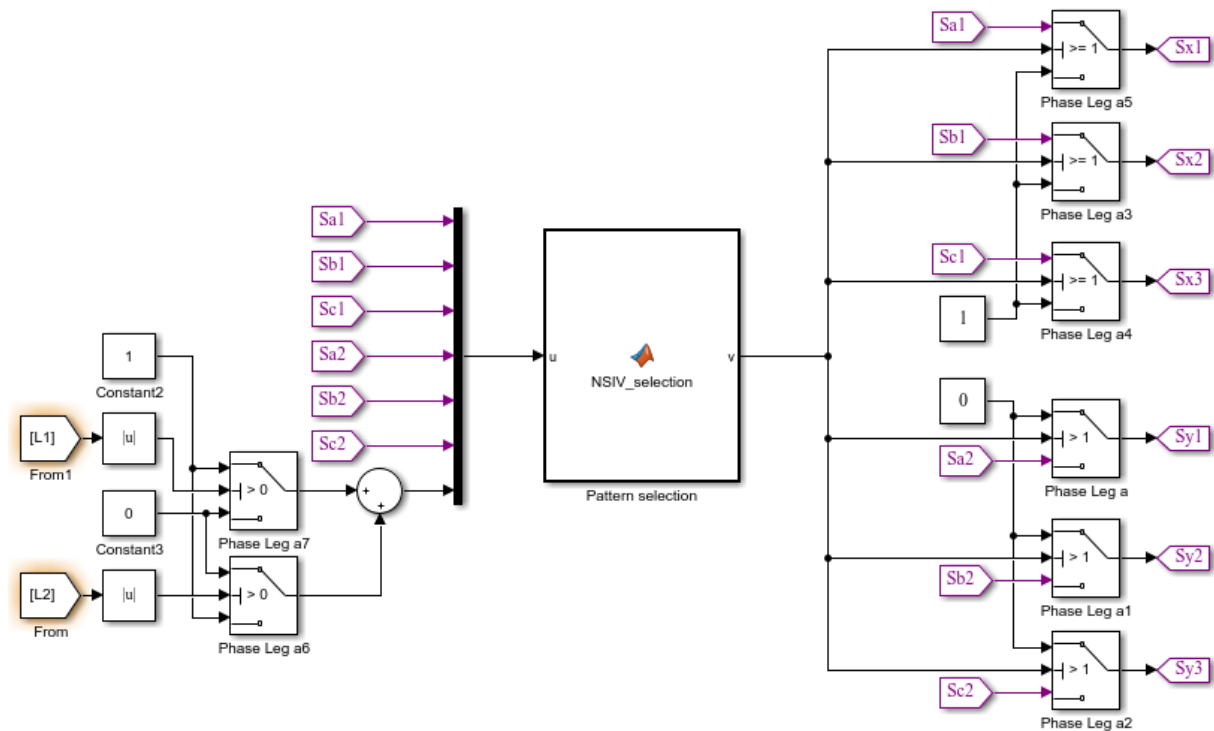


Figure III.8. Simulink model of the synchronization block.

III.3.2. SIMULATION RESULTS

In order to demonstrate the independent control of both motors and to investigate the validity of the proposed algorithm, a simulation using the MATLAB/Simulink software is carried out (Figure III.9 presents the developed simulation model). In order of comparison with previous results (DTC with six-phase VSI), the simulation will undergo the same conditions. As well as same speed references and resistive torque load combinations. The results are illustrated in Figure III.10.

Thanks to simultaneous supply of loads, a higher acceleration has been produced and a good tracking has been obtained, the coupling of loads has not resulted in a steady state error in the speed of motors, which proves the good tracking of the suggested control scheme. Figure III.10 (a) show the speed response of motors versus the speed reference values.

There are noticeable ripples in torque response for both motors with the torque ripples of the first load being slightly larger than those of the second load due to the difference in speeds. Nevertheless, the torque ripples are still in an acceptable range.

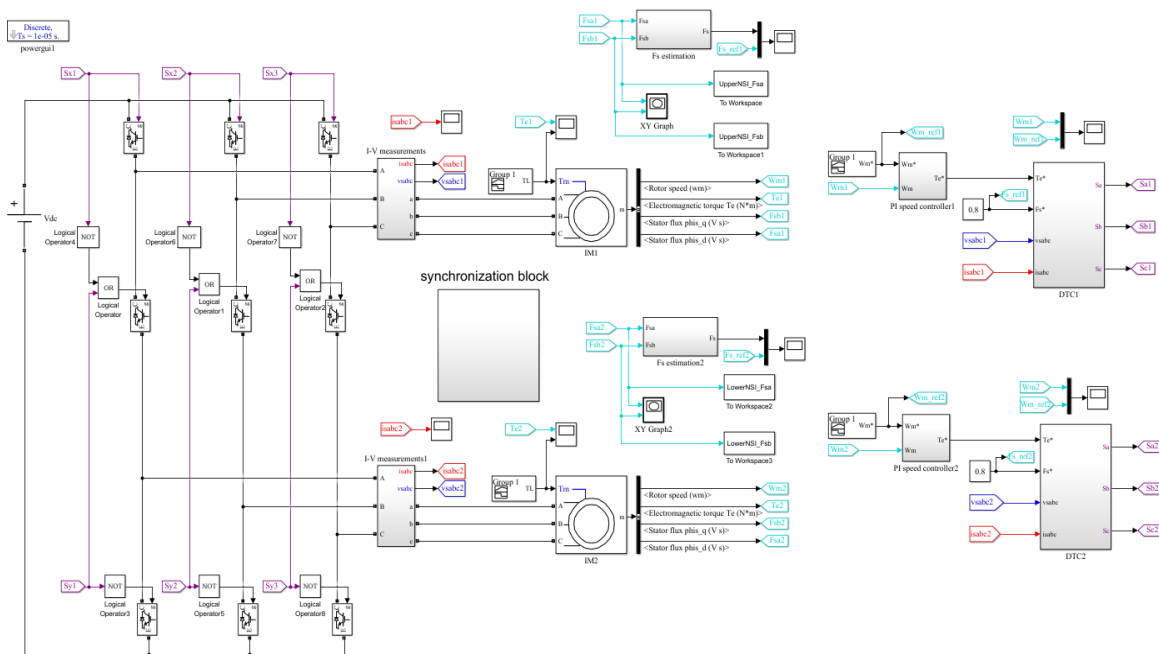


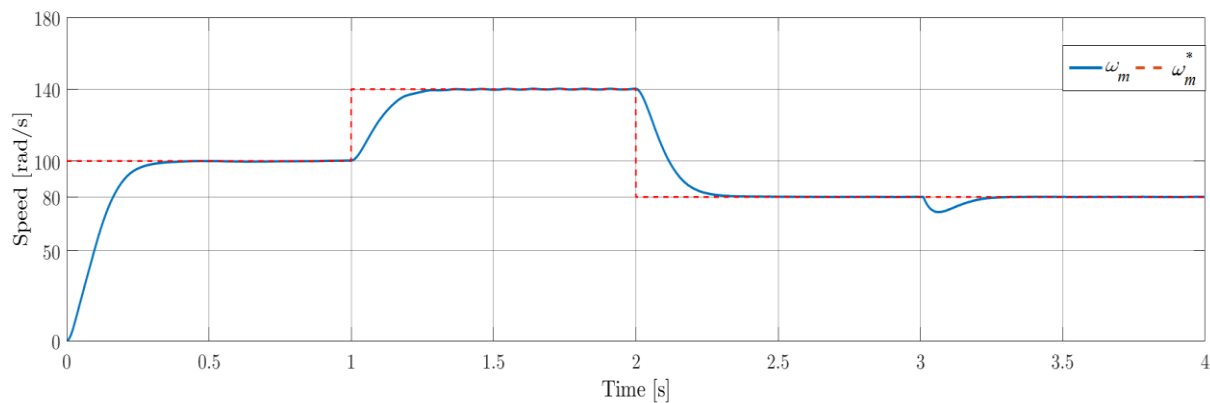
Figure III.9. Developed simulation model of DTC with NSI

The motor’s speed is regulated via the torque, using a PI controller; therefore, the motor’s reference torque increases proportionally with the acceleration requested regardless of the torque reference value at that instant, these facts justify the abrupt rise in torque when acceleration of any of the two motors is requested. Figure III.10 (b) shows Motor 1 and 2 torques vs their references values.

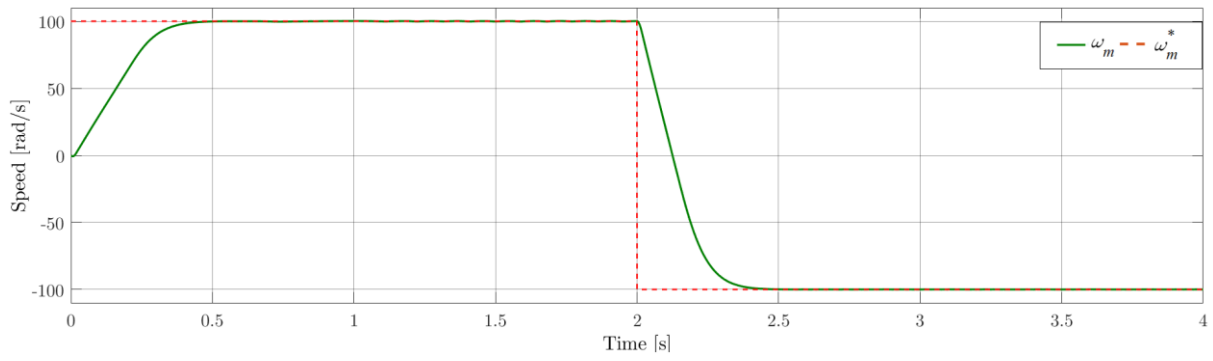
Figure III.10(c) show good reference tracking with minimum stator flux ripples for each motor, which is translated to circular locus depicted in Figure III.10 (e).

(a) Rotational speed

IM1

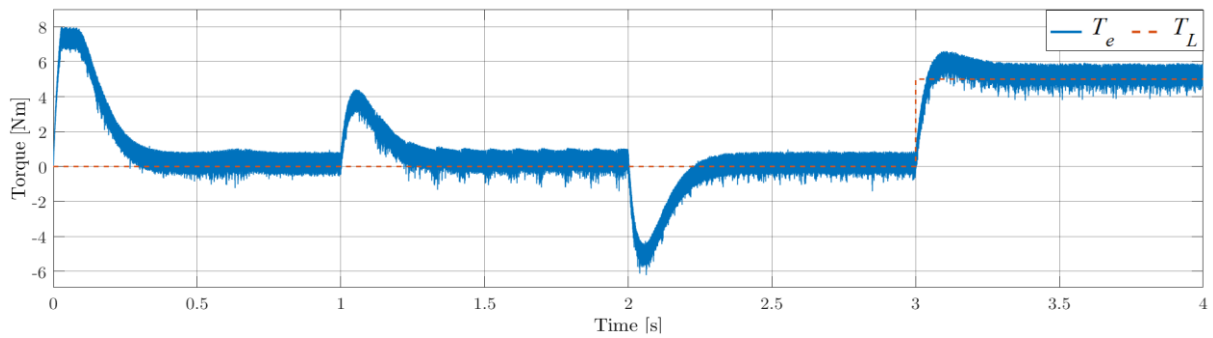


IM2

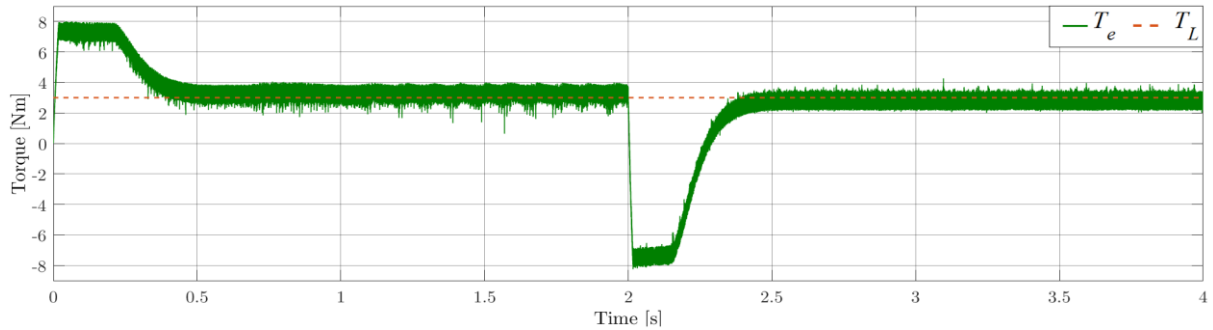


(b) Electromagnetic torque

IM1

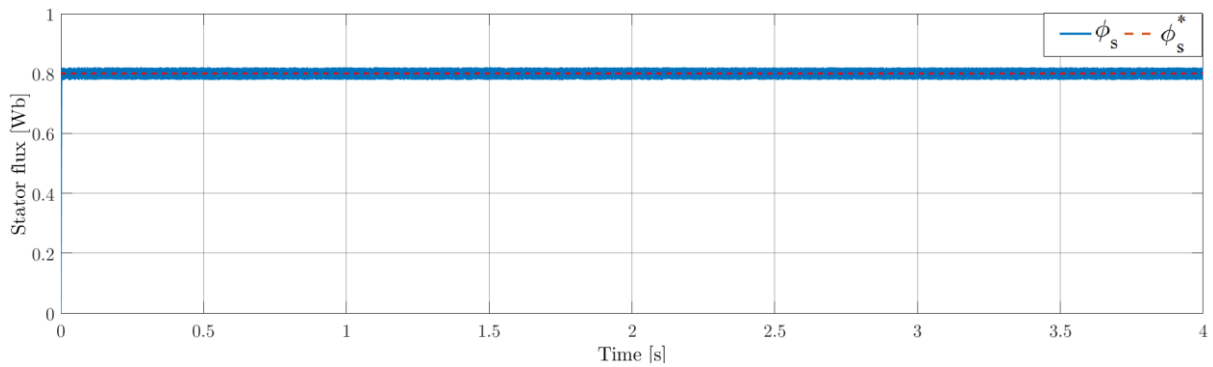


IM2

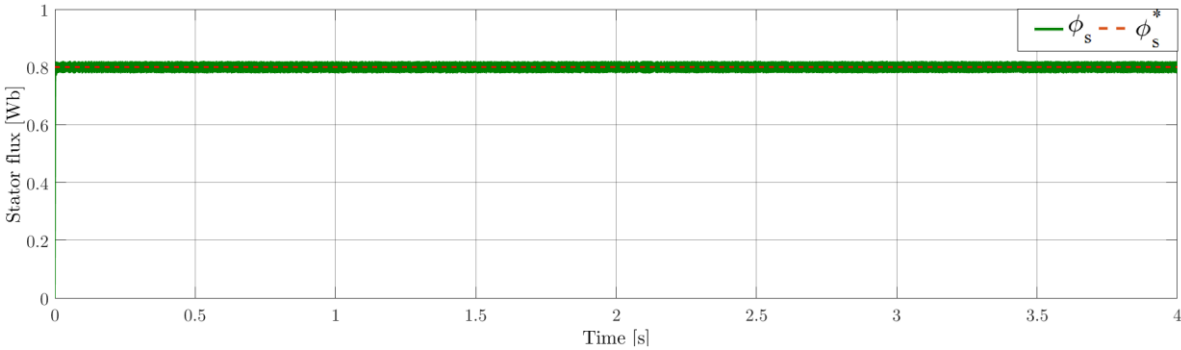


(c) Stator flux

IM1

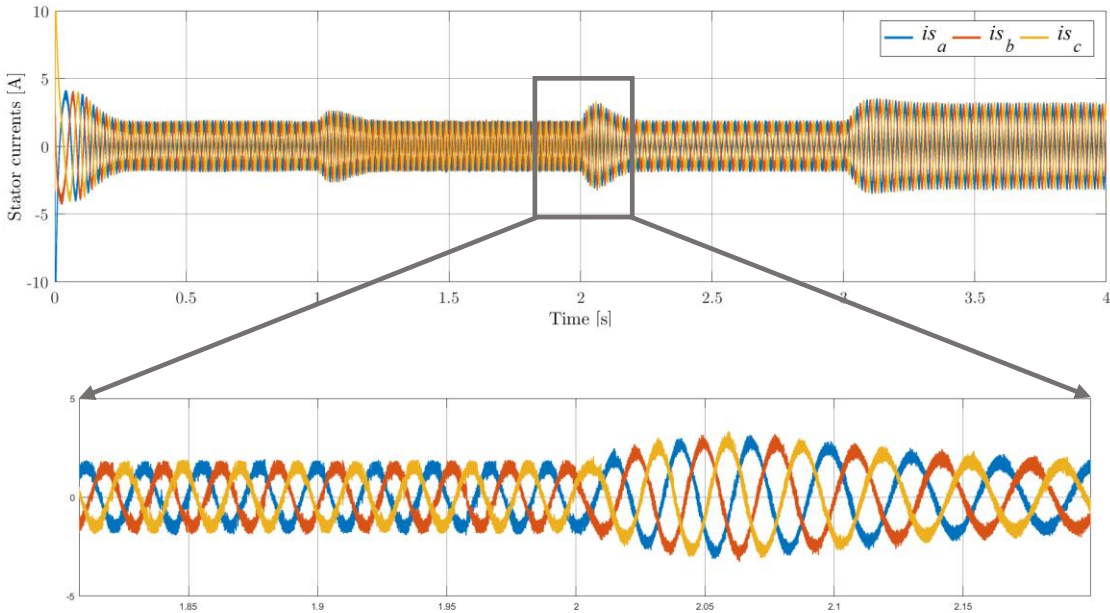


IM2

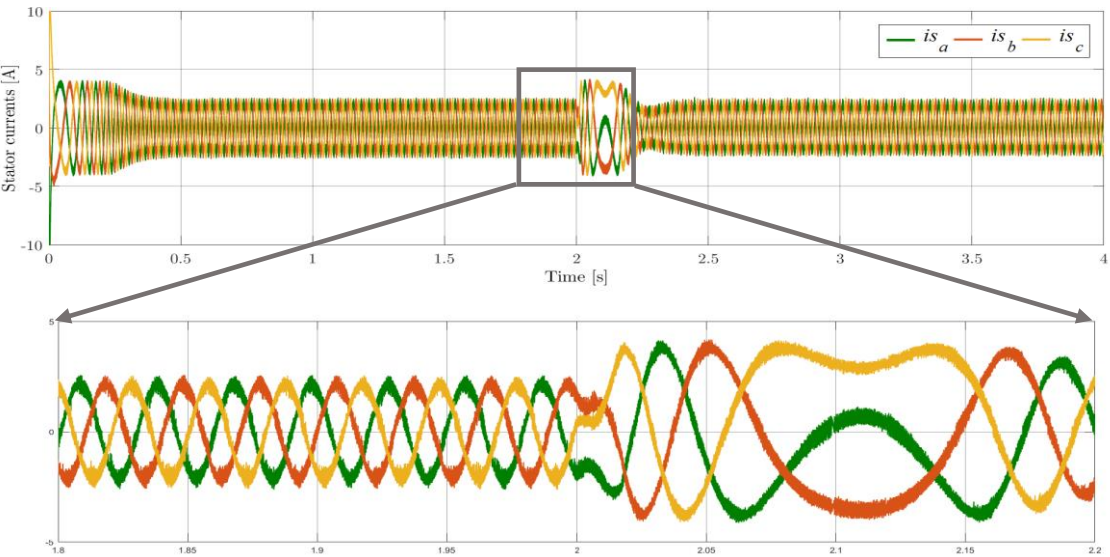


(d) Stator current

IM1



IM2



(e) Stator flux trajectory

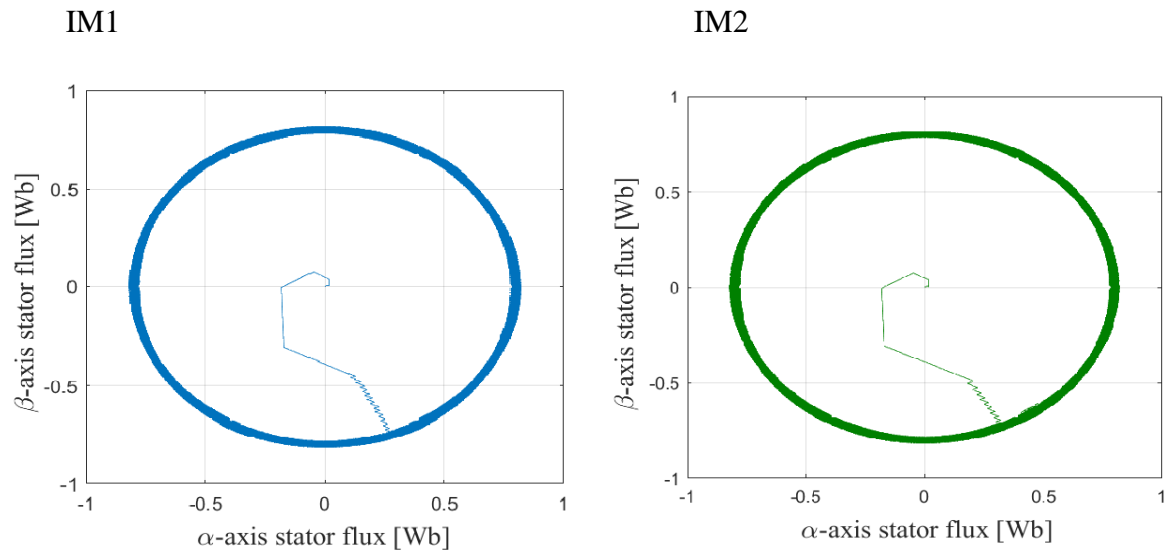


Figure III.10. Simulation results of DTC with NSI for several speed combinations coupled with nominal loads.

III.4. COMPARATIVE STUDY

For a fair and good comparison between DTC with NSI and DTC with six-phase VSI. Tables III.1 and III.2 were drawn that includes figures of zoomed-in results from simulation of the torque, flux, and the stator current of the phase (a), and the ‘THD’ of the latter, the figures captured from both approaches are of the same time interval and under the same simulation conditions for both IMs.

As seen, there are no significant differences in the magnitudes of the rotor flux trajectory between the two approaches, with the NSI being slightly higher. The current waveforms of both motors from both NSI and six-phase VSI are also quite similar. As for the torque, ripples of motor 2 were similar as well, the only noticeable difference was the torque ripples of motor 1 which had higher amplitude in the NSI than six-phase VSI.

The overall performance of the NSI was close of that of the six-phase VSI. Nevertheless, the reduced switches and overall cost of the NSI should make a compelling argument in its favor.

Table III. 1. Comparison between both approaches Motor 01 (Blue).

	DTC with NSI	DTC with six-phase VSI
Flux waveform		
Torque waveform		
Phase current (a)		
THD (%) current (a)	11.60	10.51

Table III. 2. Comparison between both approaches Motor 02 (Green).

	DTC with NSI	DTC with six-phase VSI
Flux waveform		
Torque waveform		
Phase current (a)		
THD (%) Current (a)	9.73	8.83

III.5. CONCLUSION

In this chapter, DTC schemes with both structures of the nine-switch inverter as well as six-phase voltage source inverter that consists of two separate two-level inverters were presented. A simple and effective algorithm is suggested to control the NSI using the DTC control scheme. Simulation results illustrate the independency in control and simultaneous supply of the two motors using the suggested algorithm. Finally, comparative discussion was held, to further demonstrate the validity of the suggested control method and solidify the viability of the nine-switch inverter as a substitute to the conventional six-phase voltage source inverter for dual output application.

General Conclusion

The work presented in this dissertation aims to design a dual output inverter with a complete independency in control of two induction motors. For this, several structures were presented with emphasis on the configuration of a nine-switch inverter (NSI). In this structure, only nine switches are used (three switches per leg) rather than twelve switches in the classical six-phase voltage source inverter (VSI). This configuration minimizes the number of components of the power electronics and therefore minimizes the cost and volume of the drive system.

In this work, a general study of induction motor, voltage source inverters both six-phase VSI and the nine-switch inverter were presented as well as basic principle and operation of DTC, which were backed by simulations carried out on the Matlab/Simulink software.

Furthermore, the general structure of six-phase VSI with the use of DTC scheme was discussed followed by simulation results. A simple and effective algorithm is suggested to control the NSI using the DTC control scheme, again simulation studies have been carried out on the Matlab/Simulink software, which proved the validity and efficiency of the direct torque control method with the proposed algorithm applied to the nine-switch inverter supplying two induction motors.

To finalize, a comparison between the use of DTC with the classic six-phase VSI and the suggested method with NSI was the subject of discussion. Concluding and in brief, thanks to the simultaneous supply of motors ensured by the new algorithm acceptable results were achieved.

As perspective to this work, we propose the following:

- Using the nine-switch inverter in an electric vehicle application by implementing advanced control techniques.
- Work is needed to improve torque and flux ripples.
- Real world implementation of the suggested control technique should be interesting.

Appendix

The parameters of the squirrel cage induction motor used in this work are described in the table below

<i>Machine's Power</i>	<i>1.1 KW</i>
<i>Stator resistance</i>	$R_s = 6.75 \Omega$
<i>Rotor resistance</i>	$R_r = 6.21 \Omega$
<i>Stator inductance</i>	$L_s = 0.519 \text{ H}$
<i>Rotor inductance</i>	$L_r = 0.5192 \text{ H}$
<i>Mutual inductance</i>	$M_{sr} = 0.4957 \text{ H}$
<i>Number of pole pairs</i>	$p = 2$
<i>Friction coefficient</i>	$f = 0.002 \text{ SI}$
<i>The moment of inertia</i>	$j = 0.01240 \text{ kg.m}^2$
<i>Rated voltage</i>	$V_s = 220/380 \text{ V}$

Table A.1. Parameters of the induction machine

References

- [1] D. J. Rhees, "Electricity-" The greatest of all doctors": An introduction to" High frequency oscillators for electro-therapeutic and other purposes", " *Proc IEEE*, vol. 87, pp. 1277-1281, 1999.
- [2] A.I.Voldek. Electrical machines. Textbook for students of higher tech. institutions. Second edition-Leningrad: 1974.
- [3] Austin Hughes. Electric Motors and Drives Fundamentals, Types a Applications. 3rd ed. Newnes, 2006.
- [4] (Advances in Industrial Control) Alain Glumineau_ Jesús de León Morales (auth.)-Sensorless AC Electric Motor Control_ Robust Advanced Design Techniques and Applications-Springer International Publishi
- [5] Abdelghani, D.; and Boumediene, A. (2018). Direct torque control of two induction motors using the nine-switch inverter. *International Journal of Power Electronics and Drive Systems (IJPEDS)*, 9(4), 1552-1564.
- [6] Abu-Rub, H.; Iqbal, A.; and Guzinski, J. (2012). *High performance control of ac drives with MATLAB/Simulink models (1st Ed.)*. West Sussex, England: John Wiley & Sons Ltd.
- [7] G. S. Buja and M. P. Kazmierkowski, "Direct torque control of a PWM inverter-fed AC motors—A survey," *IEEE Trans. Ind. Electron.*, vol. IE-51, no. 4, pp. 744–757, Aug. 2004.
- [8] Direct Torque Control Strategies of Induction Machine: Comparative Studies By Cherifi Djamila and Miloud Yahia Submitted: 24th OF May 2019 Reviewed: October 17 2019 Published January 24 2020.
- [9] F. Blaabjerg, S. Freysson, and H. H. Hansen, "A new optimized space-vector modulation strategy for a component-minimized voltage source inverter," *IEEE Trans. Power Electron.*, vol.12, no.4, pp. 704–714, Jul. 1997.
- [10] M. Jones, S. N. Vukosavic, D. Dujic, E. Levi, and P. Wright, "Five-leg inverter PWM technique for reduced switch count two-motor constant power applications," *IET Electr. Power Appl.*, vol. 2, no. 5, pp.275–287, Sep. 2008.
- [11] T. Kominami and Y. Fujimoto, "A novel nine-switch inverter for independent control of two three-phase loads," in *Conf. Rec. IEEE IAS Annu.Meeting*, 2007, pp. 2346–2350.
- [12] A Hybrid Direct Torque Control Scheme for Dual Three-Phase PMSM Drives With Improved Operation Performance *IEEE Transactions on Power Electronics* (Volume: 34, Issue: 2, Feb. 2019).

Abstract:

Industrial applications require large numbers of motors supply; therefore, it is necessary to design system with low cost, reduced losses and higher efficiency. The nine-switch inverter is a recent reduced semiconductor topology, for dual output applications, as a substitute of two separate voltage source inverters. It can be used to drive two three-phase induction motors independently.

In this context, direct torque control method is developed to ensure the separate control of both induction motors. Simulations are carried-out to show that the developed independent control is effective and provides a simple configuration with high performance in terms of speed, torque and flux responses.

Résumé :

Les applications industrielles nécessitent l'alimentation d'un grand nombre de moteurs ; par conséquent, il est nécessaire de concevoir un système à faible coût, des pertes réduites et une efficacité plus élevée. L'onduleur à neuf commutateurs est une topologie à semi-conducteurs réduite récente, pour les applications à double sortie, en remplacement de deux onduleurs à source de tension distincts. Il peut être utilisé pour piloter indépendamment deux moteurs asynchrones triphasés.

Dans ce contexte, une méthode de contrôle direct du couple est développée pour assurer le contrôle séparé des deux moteurs à induction. Des simulations sont effectuées pour montrer que la commande indépendante développée est efficace et offre une configuration simple avec des performances élevées en termes de réponses en vitesse, couple et flux.

ملخص:

تتطلب التطبيقات الصناعية عددًا كبيرًا من المحركات؛ لذلك، من الضروري تصميم نظام بتكلفة منخفضة وخسائر منخفضة وذات كفاءة عالية. العاكس ذو التسعة مفاتيح هو طوبولوجيا حديثة منخفضة من حيث اشباه الموصلات، لتطبيقات الإخراج المزدوجة، كبديل لاثنتين من محولات مصدر الجهد المنفصلين. يمكن استخدامه لقيادة اثنين من المحركات الحثية ثلاثية الطور بشكل مستقل.

في هذا السياق، تم تطوير طريقة التحكم المباشر بالعزم لضمان التحكم المنفصل لكل من محركات الحث. يتم إجراء عمليات المحاكاة لإظهار أن التحكم المستقل المطور فعال ذو تكوين بسيط ويوفر أداء عالٍ من حيث السرعة وعزم الدوران واستجابة التدفق المغناطيسي.